



## Winter Intrusions of Atlantic Water in Kongsfjorden: Oceanic Preconditioning and Atmospheric Triggering

Francesco De Rovere<sup>1,2</sup> , Davide Zanchettin<sup>1</sup> , Angelo Rubino<sup>1</sup>, Leonardo Langone<sup>2</sup>, Francesco Calogiuri<sup>3</sup>, Paolo Ruggieri<sup>3</sup> , Angelo Lupi<sup>2</sup>, and Jacopo Chiggiato<sup>4</sup> 

### Special Collection:

The Arctic: An AGU Joint Special Collection

### Key Points:

- Sudden winter intrusions of Atlantic Water in Kongsfjorden are typically triggered by abrupt *reversals* of local meridional winds
- The dynamics of the intrusions are determined by the density difference between fjord and Atlantic waters
- The peculiar intrusion of winter 2014 was triggered by long-lasting southerly winds, transporting warm surface waters toward the fjord

### Supporting Information:

Supporting Information may be found in the online version of this article.

### Correspondence to:

F. De Rovere and L. Langone,  
[francescoderovere@cnr.it](mailto:francescoderovere@cnr.it);  
[leonardo.langone@cnr.it](mailto:leonardo.langone@cnr.it)

### Citation:

De Rovere, F., Zanchettin, D., Rubino, A., Langone, L., Calogiuri, F., Ruggieri, P., et al. (2024). Winter intrusions of Atlantic water in Kongsfjorden: Oceanic preconditioning and atmospheric triggering. *Journal of Geophysical Research: Oceans*, 129, e2023JC020095. <https://doi.org/10.1029/2023JC020095>

Received 15 JUN 2023

Accepted 29 APR 2024

### Author Contributions:

**Conceptualization:** Francesco De Rovere, Davide Zanchettin

**Formal analysis:** Francesco De Rovere

**Investigation:** Francesco De Rovere, Francesco Calogiuri, Jacopo Chiggiato

**Methodology:** Francesco De Rovere, Davide Zanchettin

**Supervision:** Angelo Rubino, Jacopo Chiggiato

**Writing – original draft:**

Francesco De Rovere

**Writing – review & editing:**

Davide Zanchettin, Angelo Rubino, Leonardo Langone, Francesco Calogiuri, Paolo Ruggieri, Angelo Lupi, Jacopo Chiggiato

<sup>1</sup>Department of Environmental Sciences, Informatics and Statistics, Ca' Foscari University of Venice, Venezia, Italy,

<sup>2</sup>Consiglio Nazionale delle Ricerche, Istituto di Scienze Polari (CNR-ISP), Bologna, Italy, <sup>3</sup>Department of Physics and Astronomy, University of Bologna, Bologna, Italy, <sup>4</sup>Consiglio Nazionale delle Ricerche, Istituto di Scienze Marine (CNR-ISMAR), Venezia, Italy

**Abstract** Kongsfjorden, an Arctic fjord in Svalbard, is largely influenced by the West Spitsbergen Current (WSC), transporting warm and salty Atlantic Water (AW) into the Arctic region. Despite the geostrophic control preventing AW from entering the fjord in winter, AW intrusions occasionally occur during energetic local wind events in this season. However, recent intrusions remain poorly characterized, and the underlying mechanism(s) and large-scale precursors are only partly understood. This study uses in-situ oceanographic and atmospheric measurements, alongside reanalysis data covering 2011–2020, to describe recent wintertime AW intrusions in Kongsfjorden. By discerning common traits in the observed events, the main triggering factors and controls of the phenomenon are described. Our results indicate that AW intrusions are typically triggered by wind *reversals* over the shelf, consisting of the sudden transition from a strong southerly to a northerly circulation linked to the setup and damping of a high-pressure anomaly over the Barents Sea. Ocean density is a critical preconditioning factor influencing the nature of the intrusion: when fjord waters exhibit a lower density compared to WSC waters, wind *reversals* induce AW intrusions by upwelling; in contrast, when fjord waters present higher or similar densities compared to WSC waters, *reversals* force AW inflows near the surface or at intermediate depths, respectively. Another mechanism was observed only in winter 2014: southerly winds prevailed for 2 months, transporting surface AW from the WSC into the fjord, promoting its intrusion near the surface, on top of denser local waters.

**Plain Language Summary** Kongsfjorden, an Arctic fjord in Svalbard, is largely influenced by the WSC, which carries warm and salty Atlantic Water (AW) into the Arctic region. Occasionally, the fjord experiences sudden wintertime warming events due to intrusions of AW, whose underlying mechanism(s) and large-scale precursors remain only partly described. By examining events observed in the 2011–2020 decade, we found that changes in wind direction typically trigger such intrusions, precisely when energetic winds from the south are followed by winds from the north. These episodes lead to abrupt warming events, but AW intrusions occur only when the density of the fjord is lower than that of the WSC. When fjord waters have a similar or larger density than WSC waters, wind events generate AW inflows at intermediate or near-surface depths, respectively. Hence, the atmosphere triggers the AW intrusion, but its dynamics are determined by oceanic conditions, acting as a critical preconditioning factor. Additionally, a second intrusion mechanism was observed: prolonged winds from the south force AW from the WSC to intrude in the near-surface layers of the fjord, on top of denser waters.

## 1. Introduction

The Arctic is acknowledged as a “climatic hotspot” by the scientific community (Meredith et al., 2019). Since the 1960s, Arctic near-surface air temperatures are increasing at a higher rate compared to the global average, a process named *Arctic amplification* (Chylek et al., 2009; Richter-Menge & Druckenmiller, 2020; Serreze & Barry, 2011), sustained by the loss of Arctic sea-ice volume (Carmack et al., 2015; Comiso, 2012) and the *ice-albedo feedback* (Curry et al., 1995). The Eurasian Arctic is subjected to *Atlantification*, that is, a gradual transition toward conditions proper of the Atlantic domain (Lind et al., 2018; Polyakov et al., 2017). An enhanced upward flux of heat and salt is deteriorating the stratification of the water column, which features fresh and cold Arctic Water (ArW) at the near-surface and warmer, saltier Atlantic Water (AW) at intermediate layers. This

process has significant implications, including enhanced sea ice melting, warming of the lower atmosphere, modifications in air-ocean interactions and ecosystem structure (Ingvaldsen et al., 2021).

The Svalbard archipelago is located in the Eurasian Arctic at the eastern side of Fram Strait, the main gateway of AW to the central Arctic Ocean. The hydrography of Svalbard is predominantly influenced by two key currents in the region: the West Spitsbergen Current (WSC) and the Spitsbergen Polar Current (SPC) (Figure 1). The WSC exhibits a strong seasonality, with peak AW transport occurring in late autumn and early winter (Beszczynska-Möller, Fahrbach, Schauer, & Hansen, 2012; Walczowski & Piechura, 2011). This current comprises two branches: the eastern branch is barotropic, while the flow in the western branch is more baroclinic. The barotropic branch is confined to the upper continental slope, on the shelf break, and conveys AW northward (Walczowski & Piechura, 2007). Properties and structure of the WSC undergo significant inter-annual variability linked to oceanic and atmospheric circulation patterns over the North Atlantic (Chatterjee et al., 2018; Muilwijk et al., 2018; Raj et al., 2018; Wang et al., 2020). The SPC (Helland-Hansen & Nansen, 1909) flows northward on the West Spitsbergen Shelf (WSS), parallelly to the WSC, and is characterized by cross-shelf sloping isopycnals, revealing its geostrophic nature (Svendsen et al., 2002). The SPC travels close to the West Spitsbergen coast and carries ArW and sea ice from Storfjorden and the Barents Sea.

Several broad fjords, that is, Kongsfjorden, Isfjorden, Bellsund, and Hornsund, are located along the western side of Spitsbergen. Kongsfjorden (Hop & Wiencke, 2019), the northernmost broad fjord in West Spitsbergen, is connected with WSC waters through a deep trough named Kongsfjordrenna. During autumn and winter, Local Water (LW) is produced in the fjord through surface heat loss, surface water densification, and convection, resulting in temperatures smaller than 1°C. ArW flows on the shelf and mixes with AW to form Transformed Atlantic Water (TAW) (Tverberg et al., 2019). In the fjord, occasional winter intrusions of AW and TAW occur, causing large positive temperature and salinity anomalies. Tverberg et al. (2019) defined AW in Kongsfjorden as water with temperature and salinity larger than 3°C and 34.9, respectively.

A geostrophic control mechanism prevents shelf waters from entering the fjord, especially during the winter season (Cottier et al., 2005; Klinck et al., 1981; Svendsen et al., 2002). The degree of control is determined by the strength of the SPC, depending primarily on the shelf-fjord density gradient. When the density in the fjord is larger than that on the shelf, the strength of the coastal current increases with depth. This condition is typical of winter months when heat loss to the atmosphere and sea-ice production increase density in the deep fjord basin. As a result, AW advected near the bottom through Kongsfjordrenna joins this coastal current at the fjord mouth, making a detour northward. On the opposite, when shelf waters are denser than fjord waters, typically in summer months due to large amounts of freshwaters discharged from local glaciers, the speed of the coastal current decreases with depth. The geostrophic control mechanism breaks down and WSC waters are free to enter the fjord at intermediate and large depths, while the coastal current is confined in the upper layers.

Density fluctuations on the shelf develop horizontal pressure gradients between the fjord and the shelf, driving baroclinic currents (Klinck et al., 1981; Stigebrandt, 1981; Svendsen, 1980). Such fluctuations result from water convergence and divergence near the coast generated by wind stress curl and Ekman transport, causing downwelling and upwelling, or by advection of horizontal density gradients along the coast. Strong southerly winds and a negative wind curl over the WSS can stack up low-density surface waters along the coast. Once the wind ceases, the water column on the shelf returns to a normal stratification state and the fjord adjusts to it with an outflow near the surface and an inflow near the bottom. Episodes of this “intermediary circulation” have been observed also in Greenland fjords (Jackson et al., 2014; Straneo et al., 2010). Wind events on the shelf may also lead to geostrophic advection of WSC waters into West Spitsbergen fjords through the development of the Spitsbergen Through Current (STC) (Nilsen et al., 2016). Water convergence near the coast reinforces the positive gradient in surface tilt over the shelf break. Consequently, both the WSC and the SPC strengthen (Teigen et al., 2010), causing the WSC to shift toward shallower isobaths on the WSS, generating the topographically guided STC. Subsequent northerly winds initiate upwelling of the STC on the shelf. Nilsen et al. (2016) and Cottier et al. (2007) suggest that the resulting southward surface current on the shelf opposes the SPC, potentially disrupting the geostrophic control mechanism and allowing the STC to intrude into West Spitsbergen fjords. The strong southerly wind events described by Nilsen et al. (2016) are generated by the passage of the so-called winter cyclones. Strong blocking conditions developing over Scandinavia and Europe stretch the Atlantic storm track over the Greenland Sea toward the Arctic (Häkkinen et al., 2011; Rogers et al., 2005; Ruggieri et al., 2020), generating southerly winds over the eastern Fram Strait and the arrival of warm and humid air masses over Svalbard. Other effective

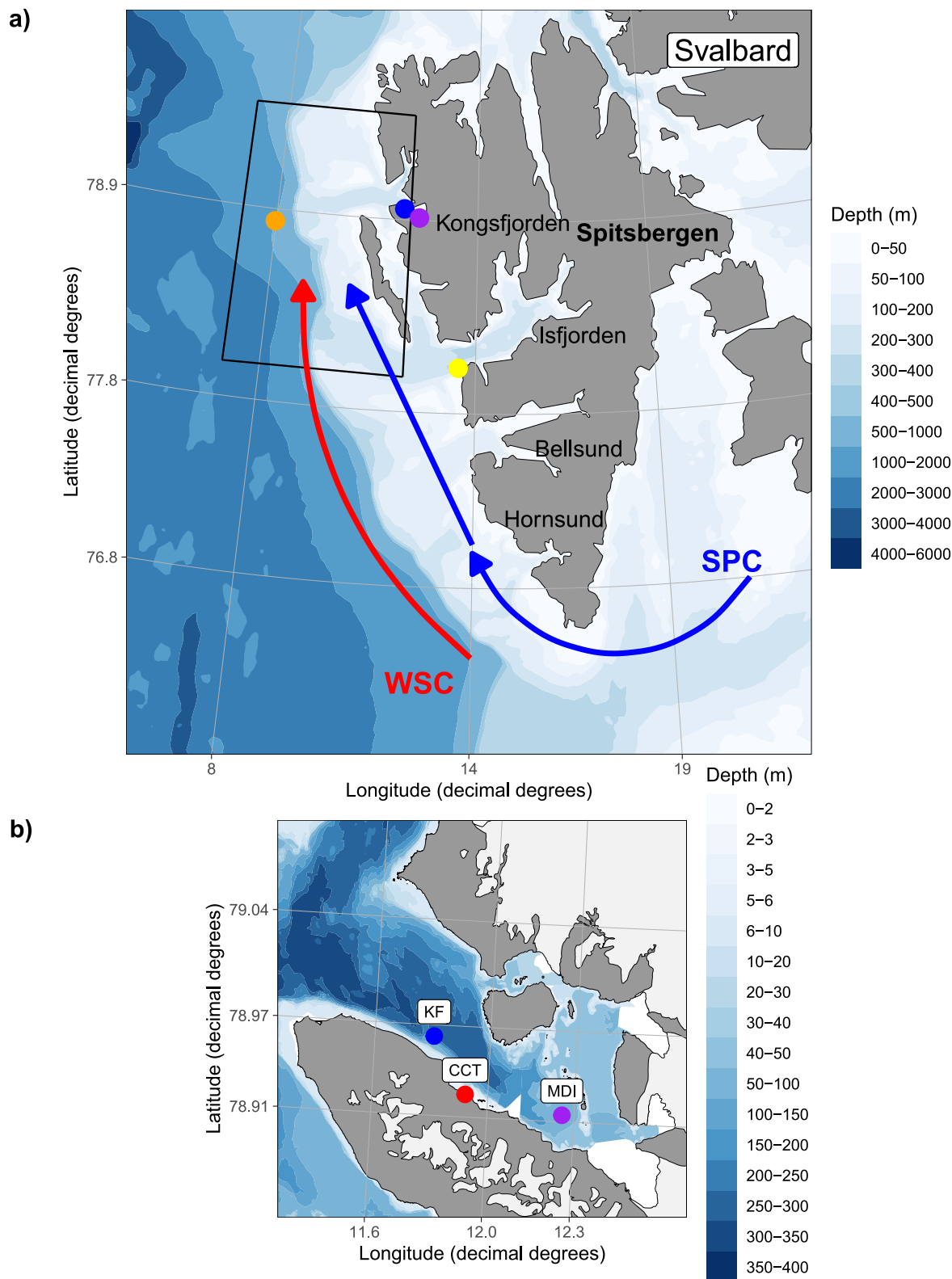


**Figure 1.** (a) Map of West Spitsbergen showing the main Arctic (blue) and Atlantic (red) water currents. The four colored points indicate the location of the four moorings used in this study: MDI (purple), KF (blue), I-S (yellow), and F3 (orange). The black box highlights area A1, where ERA5 wind data are evaluated. (b) Kongsfjorden and locations of MDI, KF and Climate Change Tower. The color scales illustrate the bathymetry. This figure was generated using the PlotSvalbard R package (Vihtakari, 2020).

means of shelf-fjord exchanges are instabilities at the WSC-SPC front, developing topographic waves (Nilsen et al., 2006; Teigen et al., 2010, 2011). Stable topographic waves are generated by wind events at the shelf-edge front and can develop coastally trapped waves traveling along isobaths on the steep southern side of Kongsfjordrenna (Inall et al., 2015).

Tverberg et al. (2019) differentiate the character of the wintertime AW intrusion in Kongsfjorden in three Winter Scenarios. The *Winter Intermediate* scenario exhibits winter convection limited to intermediate depths, with AW advection occurring near the seafloor. Furthermore, shelf waters tend to spread westward above the denser WSC. The *Winter Open* scenario involves the convection of advected AW near the surface throughout the water column. Moreover, *Winter Open* features the WSC reaching the surface and spreading on the shelf at shallow levels, due to its lower density compared to shelf waters. The *Winter Deep* scenario presents winter convection extending throughout the whole water column, with no or limited AW advection in the intermediate layers. *Winter Deep* is characterized by a narrow WSC confined to the shelf edge and little exchange with the shelf.

*Atlantification* is leaving its footprint on West Spitsbergen fjords by increasing their water temperatures and salinities (Bloszkina et al., 2021; Cottier et al., 2019; De Rovere et al., 2022; Skogseth et al., 2020; Strzelewicz et al., 2022; Tverberg et al., 2019). After 2006, winters became more Atlantic-like with no sea ice and occasional shallow AW advection (Tverberg et al., 2019). Furthermore, the occurrence of intense winter cyclones passing over Svalbard is increasing (Zahn et al., 2018), potentially boosting winter AW advection on the WSS and adjacent fjords. Increasing heat content in Kongsfjorden affects also the stability of the ecosystem's structure (Hegseth & Tverberg, 2013; Payne & Roesler, 2019; Vihtakari et al., 2018) and tidewater glaciers (Holmes et al., 2019; Luckman et al., 2015). Henceforth, unraveling the dynamics of wintertime AW intrusions is essential to fully understand ongoing changes in Kongsfjorden and the future evolution of this system, especially under the influence of *Atlantification* and *Arctic amplification*.

To the best of our knowledge, a clear examination of wintertime AW intrusion events in the fjord after the 2006/2007 event is lacking. In addition, there is a need to robustly define common traits, especially the large-scale atmospheric and oceanic settings leading to AW winter intrusions. Despite being a very important factor driving dynamics on the WSS, a profound understanding of the SPC's influence on the variability of winter water masses in Kongsfjorden is still to be achieved (Tverberg et al., 2019). The scientific community now has access to in-situ continuous measurements acquired over the 2011–2020 decade from several mooring lines in the West Spitsbergen area. Exploiting the availability of such an extensive data set and high-resolution reanalysis products (ERA5) allows us to perform a comprehensive study of the typical mechanisms leading to AW winter intrusions in Kongsfjorden. Furthermore, oceanographic observations in Kongsfjorden are not just describing current conditions and ongoing changes in the fjord itself but can be indicators for the other West Spitsbergen fjords as well as for similar shelf-fjord systems in the Arctic (Bischof et al., 2019).

This work aims to investigate winter (January–March) AW intrusions in Kongsfjorden during the 2011–2020 decade by jointly examining local and large-scale, atmospheric and oceanic dynamics, combining in-situ and reanalysis data. The specific objectives are: to provide a concise overview of winter AW intrusions that occurred in the 2011–2020 decade in Kongsfjorden and to assess the dynamics of such events.

This paper is organized as follows: Section 2 provides an overview of the data utilized in this study and the methods for data analysis. Section 3 presents the results and Section 4 discusses the main findings. Section 5 provides a summary and illustrates the main conclusions of this study.

## 2. Data and Methods

### 2.1. Data

#### 2.1.1. In-Situ Data

In-situ oceanic observations in Kongsfjorden are retrieved by two moorings: MDI and KF. MDI, managed by the Institute of Polar Sciences of the National Research Council of Italy (CNR-ISP), is anchored at approximately 105 m depth in inner Kongsfjorden (78° 55'N–12° 15'E). Since September 2010, it has been monitoring temperature and salinity at 85 m with a SeaCat SBE16 (D'Angelo et al., 2018; De Rovere et al., 2022). KF is located in the mid-fjord on the southern side (78° 57.75'N–11° 48.30'E) since 2010, anchored at approximately 260 m depth and managed by the University of Tromsø (UiT) in collaboration with the Scottish Association for Marine

Sciences (Sundfjord et al., 2017). KF is situated approximately 10 km far from MDI. A continuous temperature and salinity record from a Seabird SBE37 MicroCAT sensor is available from 2010 to 2018, except for 2012, at the near-bottom (the sensor's depth ranges from 201 to 238 m). Additionally, KF has been supplied with a Seabird 16plus sensor and Minilog temperature sensors at five or more depths, enabling the representation of temperature along the water column. Furthermore, KF features two ADCPs providing current data. Ocean current observations acquired at 30-minute intervals are vertically averaged in the near-surface (20–85 m) and near-bottom (140–210 m) layers at an hourly interval. A tidal model was fitted to these current averages, with sine and cosine components corresponding to the “standard” tidal frequencies indicated in Foreman (1978), and then removed from the two series. The resulting de-tided hourly series were averaged at a daily interval and then filtered with a 3-day moving average. In this work, we utilize MDI and KF oceanographic data to define and compare the characteristics of AW intrusions in the mid-fjord and inner-fjord environments.

The University Center in Svalbard (UNIS) maintains the I-S mooring, located at the southern end of Isfjorden's mouth and anchored at approximately 205 m depth (Skogseth et al., 2020). Temperature and salinity observations obtained from a SeaGuard instrument in the near-bottom layer (179–200 m depth interval) were examined to depict conditions on the shelf adjacent to Isfjorden.

The Alfred Wegener Institute, Helmholtz Center for Polar and Marine Research (AWI), has been running a monitoring program composed of a mooring array positioned in Fram Strait since the late 1990s (Beszczynska-Möller, Fahrback, Schauer, & Hansen, 2012). The F3 mooring, positioned near the shelf break (78.83°N–8°E) at 1,000 m depth, provides temperature and salinity data collected by an SBE37 sensor in the intermediate layer (250–300 m depth), describing properties of the western off-shore WSC edge.

Meteorological conditions in Kongsfjorden were inspected through observations acquired by a Vaisala thermohygrometer and a Young Marine wind sensor installed at 10 m height on the Climate Change Tower (CCT) in the village of Ny-Ålesund (Mazzola et al., 2016), on the southern side of the fjord.

All in-situ observations were acquired at frequencies of 10, 20, 30 or 60 minutes. Raw data were checked to remove spikes and inaccurate observations. Eventually, all observations were averaged at a daily interval.

### 2.1.2. Reanalysis Data Sets

Winds at 10 m height and geopotential height fields at 850 hPa over the Arctic and Fram Strait regions were analyzed to describe large-scale atmospheric conditions. Hourly data were retrieved from ERA5 reanalyses (Hersbach et al., 2023a, 2023b) and then averaged at a daily interval. In addition, monthly average products of geopotential heights were utilized (Hersbach et al., 2023c). Wind and wind stress curl data were averaged over an area representative of the WSS adjacent to Kongsfjorden (A1, black rectangle reported in Figure 1a; 7–12°E, 78–79.5°N), and smoothed with a 3-day moving average. Wind stress and wind stress curl were calculated as in Goszczko et al. (2018) and through the oce R package (Kelley & Richards, 2022), respectively. Daily salinity fields at 50 m depth from the CMEMS Arctic Ocean Physics Reanalysis (TOPAZ4) (Sakov et al., 2012; Xie et al., 2017) with a spatial resolution of 12.5 × 12.5 km were used to define the large-scale oceanic conditions in the Eurasian Arctic region.

Monthly time series of climate indices for the main northern Atlantic hemispheric teleconnection patterns (Barnston & Livezey, 1987) were retrieved from the NOAA Climate Prediction Center (NOAA, 2012). These include the North Atlantic Oscillation, Arctic Oscillation, East Atlantic pattern, East Atlantic/Western Russia pattern, and Scandinavia pattern.

## 2.2. Methods

A wintertime AW intrusion event was identified through MDI temperature and salinity data. MDI is used as a reference station for two reasons. First, MDI is strategically positioned within the inner fjord, thus effectively capturing the most significant AW intrusion events. Second, MDI acquired data continuously in the 2010–2020 decade, while KF has no data for winter 2012 and from 2018. We defined such an event as an increase in temperature (T) and salinity (S) by at least 1°C and 0.1 in one week. The onset date of an AW intrusion event was defined as that day featuring a difference in temperature and salinity equal to or larger than our thresholds compared to those values observed 7 days after. We refer to the onset date as  $t_0$ . Quantitatively, the set of conditions satisfying our definition are:

$$T_{t_0+7} - T_{t_0} \geq 1^\circ\text{C}$$

$$S_{t_0+7} - S_{t_0} \geq 0.1$$

Only the event leading to the largest temperature change each winter (from January to March) was considered. The dates of such events are reported along the MDI temperature series. For each intrusion event, time series plots illustrate MDI temperature and salinity anomalies in the interval  $[t_0 - 10, t_0 + 20]$ . Anomalies are calculated by subtracting the temperature and salinity values of  $t_0$  from the two series. In addition, a T-S diagram displays observations in the interval  $[t_0 - 10, t_0 + 9]$ .

The local oceanic and atmospheric variabilities in the interval  $[t_0 - 30, t_0 + 30]$  around the onset of wintertime AW intrusions in Kongsfjorden were examined using MDI and KF temperature and salinity observations; local meteorological measurements from the CCT, that is, air temperature, relative humidity and winds at 10 m height; average wind and wind stress curl over A1; vertical temperature at KF approximated through linear interpolation among temperature observations from available depths.

Results indicate that wind *reversals* are the key factor triggering wintertime AW intrusions (see Sections 3.2 and 4.2). The meridional component of the mean wind vector,  $V$ , was calculated as the spatial average of ERA5 daily meridional wind data over the area A1. We defined wind *reversals* as a 14-day event featuring strong southerly winds in the first week ( $\bar{V} > 3$  m/s), followed by northerly winds in the subsequent week ( $\bar{V} < 0$  m/s). Wind stress, wind stress curl and geopotential height characterizing *reversals* were assessed through a Superposed Epoch Analysis (SEA) (Chree, 1912, 1913; Singh, 2006), as it allows to detect common features shared by target events against background noise. The SEA was applied to a pool of 18 *reversals* instead of considering only *reversals* associated with the observed AW intrusion (5 events) to increase the robustness and significance of our results. We created this larger pool by applying the *reversal's* definition in the 2011–2020 winters (from January to March). Superposed Epoch Analysis calculations were performed by averaging two-dimensional daily atmospheric fields observed in each *reversal's* first and second week. For the geopotential height, averages were calculated over daily anomalies, and anomalies were computed by subtracting the 2011–2020 winter climatology from the daily fields. The significance of geopotential height anomalies was calculated as follows: 18 casual dates over the 2011–2020 winters were selected, and the associated mean geopotential anomalies in the subsequent first and second weeks were calculated. We repeated this step 100 times to produce a distribution of geopotential mean anomalies observed in the first and second weeks after casual dates. We defined significant geopotential mean anomalies calculated from the pool of 18 real *reversal* events as those anomalies smaller or greater than the 10th and 90th percentile of the casual distribution of geopotential mean anomalies, respectively. The geopotential height mean anomaly is referred to as z850. z850 significance is illustrated for areas spanning  $15^\circ$  longitude and  $5^\circ$  latitude. Non-significant areas reported in the results comprise more non-significant ERA5 grid points than significant ones.

The link between *reversals* and the general atmospheric circulation was examined using a correlation analysis. A Pearson correlation coefficient was calculated between the number of winter *reversal* events per winter and the winter average (from January to March) of those monthly teleconnection indices listed in Section 2.1.2.

We assessed the fjord's oceanic response to wind *reversals* through MDI and KF measurements. Average potential temperature and potential density conditions in the first and second weeks of *reversals* were calculated, their difference computed ( $\delta\theta$  and  $\delta\rho$ ) and illustrated in a scatterplot. Similarly, average potential temperature ( $\theta$ ) and salinity conditions in *reversals'* first and second weeks were calculated and reported in a T-S diagram.

We used daily TOPAZ4 fields to examine the large-scale oceanic conditions in the Eurasian Arctic. Two subsets of salinity fields in January-February were selected, and their average was calculated at each grid point. The first subset comprises data in years with upwelling-driven AW intrusions (2011, 2012, 2018, 2020), whereas the second subset is composed of data in the other years of the decade, excluding 2014 (2013, 2015, 2017, 2019). Winter 2014 is excluded because it features a peculiar AW intrusion, assessed separately (see Sections 3.3 and 4.3). The difference between the two subsets was calculated at each grid point. The statistical significance of this difference was examined by performing a non-parametric test (Mann-Whitney-Wilcoxon) on the two subsets defining the two averages to verify if they come from the same distribution at the 99% confidence level. Locations whose differences are associated with non-significantly different subsets are marked in the results.

Monthly geopotential anomalies from ERA5 data and the Cumulative Net Zonal Display ( $X_{Ek}$ ) were used to investigate the AW intrusion event in 2014. Monthly anomalies in December 2013 and January, February and March 2014 were calculated by subtracting the monthly climatology over the 2011–2020 time period from monthly values.  $X_{Ek}$  represents the zonal distance covered by the surface Ekman layer over a certain amount of time, forced by the wind observed over the WSS.  $X_{Ek}$  was computed using the following formula from Cushman-Roisin and Beckers (2011):

$$X_{Ek} = \frac{I}{f}$$

where  $f$  is the Coriolis parameter and  $I$  is the *wind impulse*, represented as:

$$I \simeq \frac{1}{\rho_0 H} \int_{event} \tau_y dt$$

where  $\rho_0$  is the initial density (here set to 1027.85 kg/m<sup>3</sup>),  $H$  is the depth of the Ekman layer, and  $\tau_y$ , the daily meridional wind stress over A1.  $\tau_y$  was calculated as in Goszczko et al. (2018) from ERA5 wind data.  $H$  is estimated as the theoretical Ekman layer depth:

$$H = \sqrt{2K_m / |f|}$$

where  $K_m$  is the turbulent diffusivity, assumed to be 0.1 m<sup>2</sup>/s, and  $f$  is the Coriolis parameter.  $X_{Ek}$  is compared against the distance between the WSC and Kongsfjorden, and we used the geographical location of F3 and KF moorings as a reference for this distance.

As  $X_{Ek}$  varies according to the magnitude and sign of  $\tau_y$ , to compare the multi-annual variability in the WSS near-surface atmospheric winter conditions, we compared the cumulative  $\tau_y$  observed in the 2011–2020 winters.

### 3. Results

#### 3.1. Identification of Atlantic Water Intrusion Events

Six main wintertime AW intrusion events occurring in 2011, 2012, 2014, 2016, 2018, and 2020 were identified in MDI observations. These events feature large and sudden increases in water temperature and salinity (Figures 2b and 2c).  $t_0$  dates are marked by vertical dashed red lines in Figure 2a and the zero lag vertical line in Figures 2b and 2c, and are the following: 2011-03-03, 2012-02-12, 2014-01-21, 2016-01-06, 2018-02-28, 2020-02-03. The largest temperature change takes place within the first 5 days from  $t_0$ . In this time range, the greatest temperature rise occurred in 2018 (2.51°C), while the lowest in 2014 (1.1°C). Figure 2d reports a T-S diagram showing the temperature and salinity evolution in the neighborhood of each event. LW was present in inner Kongsfjorden the days before the event and was replaced by water with increasing admixture of AW.

#### 3.2. Upwelling-Driven AW Intrusions

AW intrusions in 2011, 2012, 2016, 2018 and 2020 shared analogous dynamics, discussed in Section 4, where warmer temperatures propagate from the fjord's bottom toward the surface in a few days through upwelling. Winter 2016 features several short-lived events and peculiar conditions. The winter 2018 event is reported as an emblematic example of upwelling-driven events, while the others are illustrated in Figures S1 to S4 in Supporting Information S1. The warming signal at KF (Figure 3b) precedes MDI (Figure 3a) by approximately 3–4 days in each intrusion event. Another weaker warm water intrusion occurred near mid-February 2018 near the bottom, which does not propagate toward the surface (Figure 3i) and is not visible in MDI (Figure 3a). The AW intrusion is accompanied by large outflowing current velocities near the surface (Figure 3c) and large inflowing current velocities at depth (Figure 3d), along the main fjord axis. Instead, days preceding  $t_0$  feature inflowing currents near the surface and very low velocities near the bottom. Shelf winds are primarily southerly in the week before  $t_0$  and then turn northerly in the week after  $t_0$  (Figure 3e). The average wind stress curl is largely negative before  $t_0$ , shifting to positive when KF temperature increases (Figure 3g). We name these atmospheric events wind

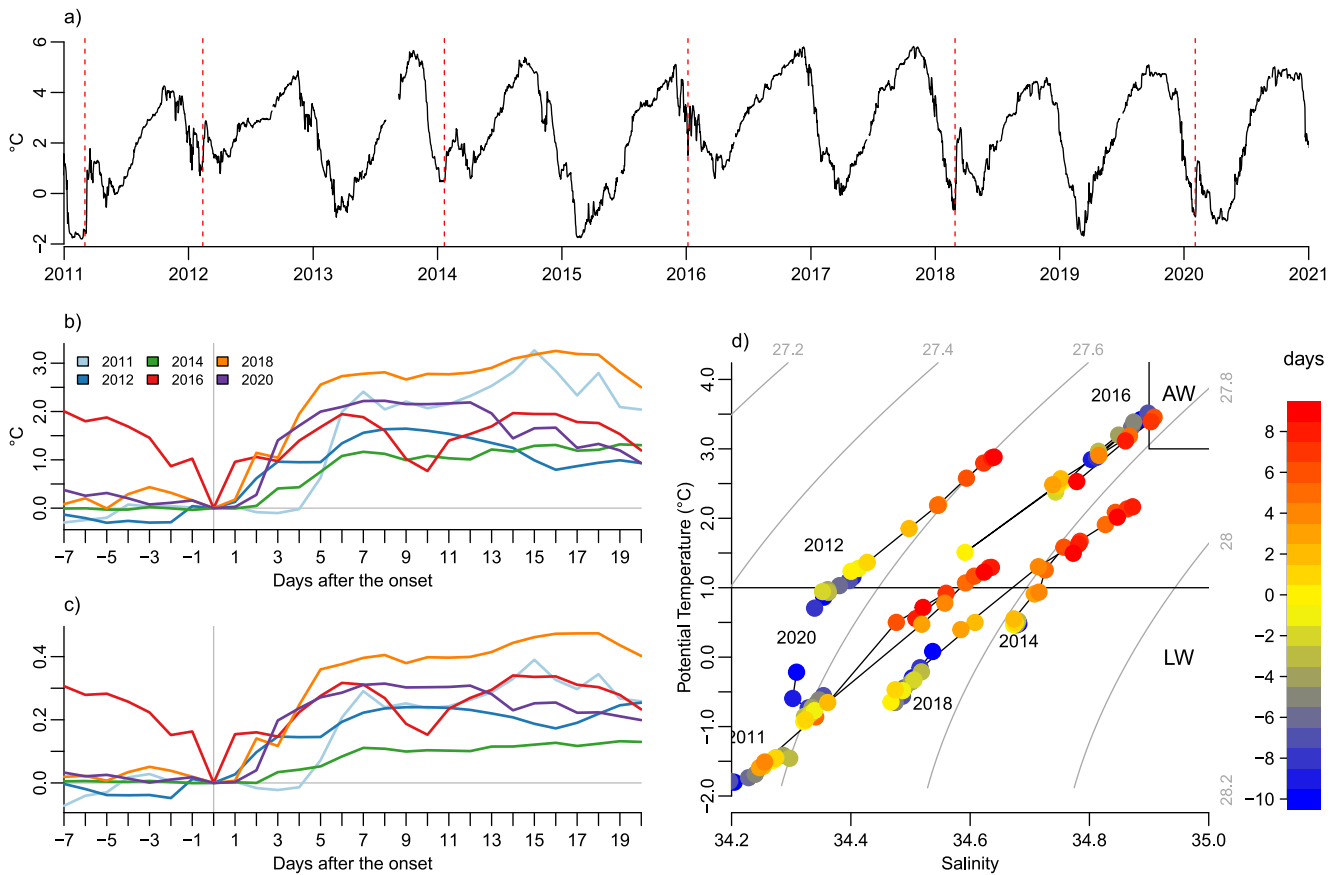


**Figure 2.** Wintertime AW intrusion events recognized from MDI observations at 85 m depth. (a) Daily temperature (black line) and identified onsets of AW intrusion events ( $t_0$ , vertical red dashed lines). Daily anomalies of (b) potential temperature and (c) salinity in the interval  $[t_0 - 10, t_0 + 20]$ . (d) T-S diagrams of measurements acquired in the interval  $[t_0 - 10, t_0 + 9]$ .

*reversals*, and Section 2.2 reports their definition. Winds in the fjord reflect the main evolution observed on the shelf (Figure 3f). Southerlies bring warm and humid air, rising air temperatures in Kongsfjorden even above 0°C, which is then replaced by cold and dry air brought by northerlies after  $t_0$  (Figure 3h).

We consider all wintertime wind *reversals* that occurred in the 2011–2020 time period (18 events), selected according to our definition (see Section 2.2), to delineate their main characteristics. The first week of wind *reversals* features strong southerly winds over the Fram Strait, resulting in upwelling in the central Fram Strait and strong downwelling on the WSS, the latter driven by the slower winds interacting with the terrain over the Svalbard archipelago (Figure 4c). In addition, this period features a high-pressure anomaly centered over the Barents Sea and a low-pressure anomaly over northern Canada and western Greenland (Figure 4a). Conversely, the second week of wind *reversals* exhibits northerly winds over the Fram Strait, initiating upwelling on the WSS (Figure 4d). This period shows negative geopotential anomalies over the north pole, the Svalbard archipelago and the northern Barents Sea, even though they are not significantly different from typical pressure conditions characterizing winter months (Figure 4b).

Oceanic conditions in Kongsfjorden during wind *reversals* reveal three noticeable features. First, not all *reversals* are followed by a significant positive temperature change, as in the case of upwelling-driven AW intrusion events. Second, the five upwelling-driven AW intrusions show the largest difference in potential density between old local waters and new inflowing waters originating from the AW intrusion (Figures 5a and 5b). Third, low-density bottom fjord waters characterize the five upwelling-driven AW intrusions in the first week of *reversals* (Figures 5c and 5d). These low-density waters result from the presence of low salinity waters (2011, 2012, 2018, 2020) or warm waters (2016) (Figures 5c and 5d).



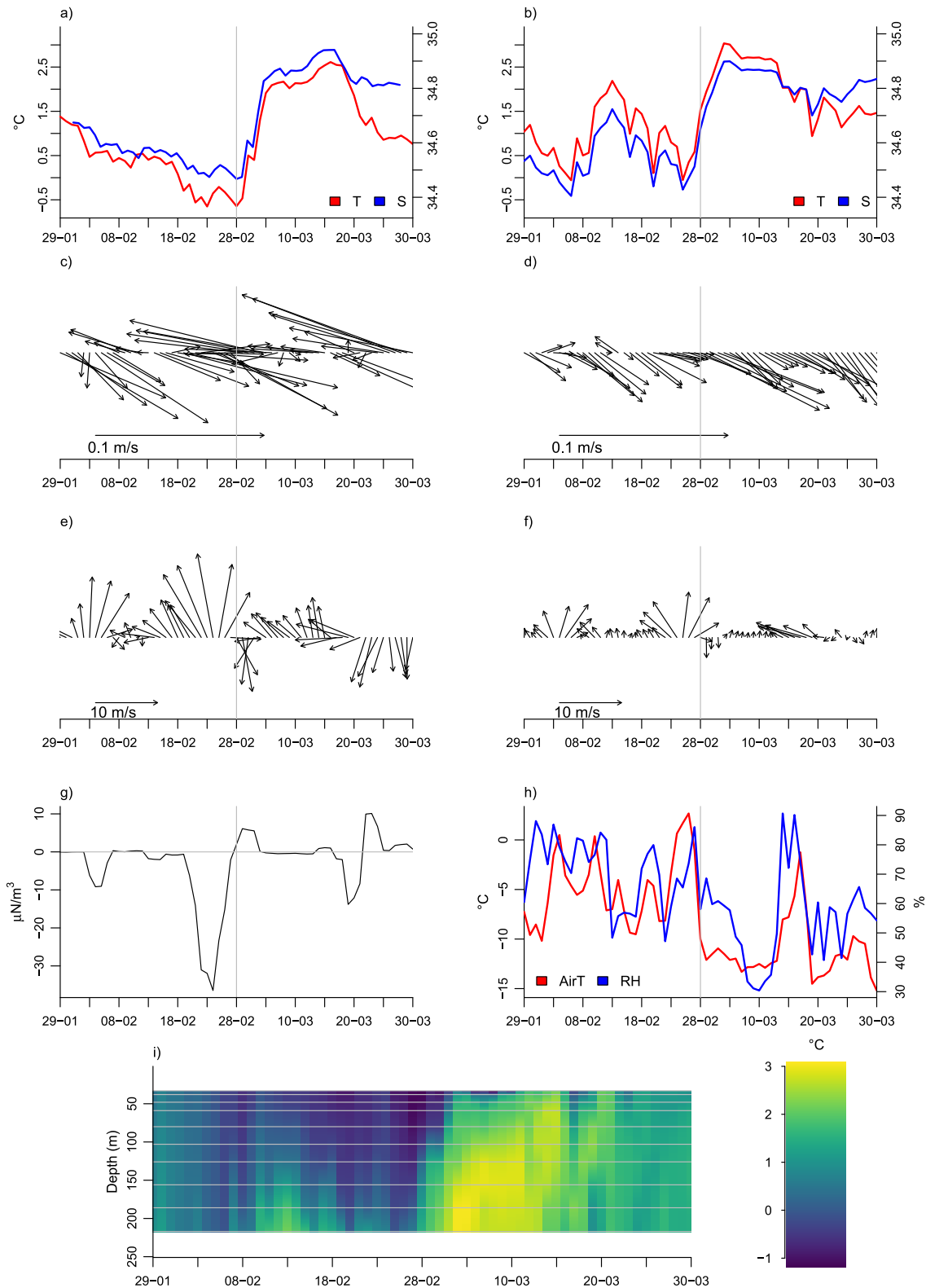


**Figure 3.** Winter 2018 as representative of upwelling-driven AW intrusion events: temperature and salinity at MDI (a) and KF (b); near-surface (c) and near-bottom (d) currents from KF; average winds (e) and wind stress curl (g) over A1 from ERA5; winds (f), air temperature (AirT, red line) and relative humidity (RH, blue line) (h) at 10 m height from the Climate Change Tower in Ny-Ålesund; (i) KF temperature profile with gray horizontal lines identifying sensors' depths. Vertical gray lines represent  $t_0$  dates.

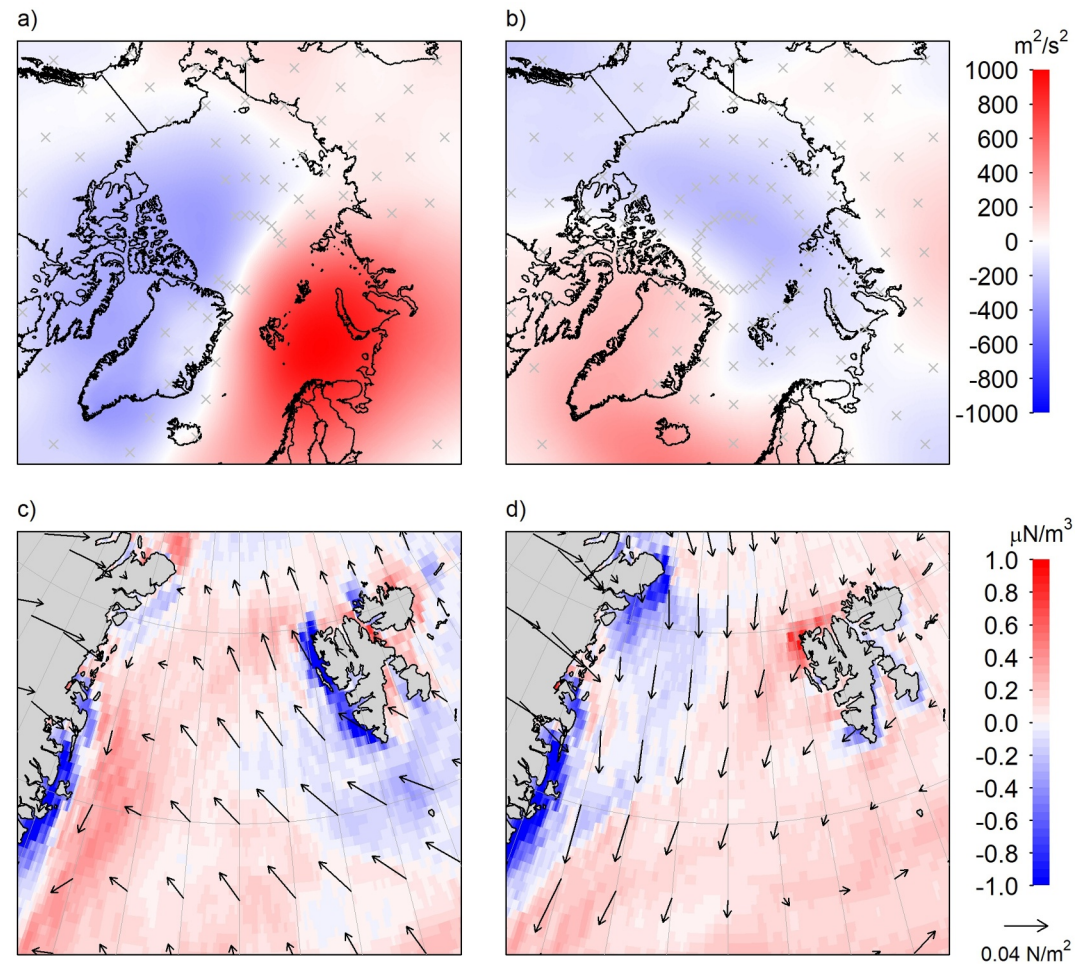


**Figure 4.** (a, b) Average geopotential anomalies at 850 hPa ( $z_{850}$ ) and (c, d) average wind stress and wind stress curl in the first and second weeks of wind reversals occurred in the 2011–2020 decade. Gray crosses in panels (a, b) identify non-significant areas (see Section 2.2 for details).

### 3.3. Downwelling-Driven AW Intrusion

The 2014 AW intrusion event shows different dynamics than the other years, that is, forced by downwelling. Warming starts from above and slowly reaches the near bottom (Figure 6i). Near-bottom sensors at KF experienced gradual warming and salinification from January to March (Figure 6b), while at mid-depth, MDI detected a sudden increase in temperature and salinity (Figure 6a). Near-surface and near-bottom currents are consistent with the arrival of shelf waters from the northwest flooding the fjord, with higher velocities at the near-surface (Figure 6c) compared to the near-bottom (Figure 6d). Shelf winds have blown predominantly from the south from January to the end of February (Figure 6e), resulting in downwelling conditions (Figure 6f). Winds in the fjord blew constantly from the south, bringing warm and humid air to Kongsfjorden (not shown).  $X_{Ek}$  shows that the theoretical Ekman layer covers the total distance between the WSC (F3 location) and Kongsfjorden (KF location) in 64 days, thus arriving in the fjord at the beginning of February 2014 (Figure 6g).

## 4. Discussion

### 4.1. Events of AW Intrusion

We identified six main AW intrusion events through MDI mooring data, representing the advection of variable mixtures of WSC waters into Kongsfjorden. Consequently, winter conditions in the inner fjord shifted from being more Arctic to more Atlantic in less than 7 days, and these conditions persisted for a few weeks. Among the six events, those in winters 2011, 2012, 2016, 2018 and 2020 exhibited consistent dynamics, with the warming signal

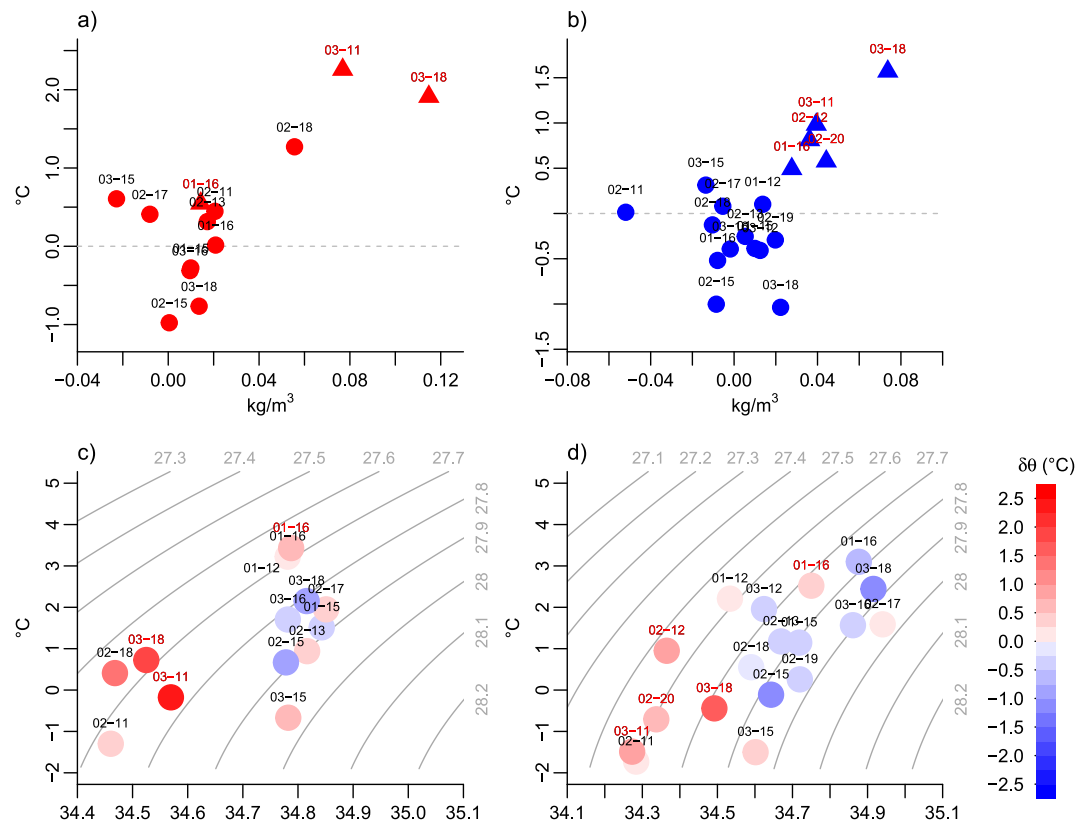


**Figure 5.** Near-bottom ocean conditions in mid (KF) and inner (MDI) Kongsfjorden during all 18 reversals identified in the 2011–2020 winters. A change in potential density ( $\Delta\rho$ ) between the first and second weeks of reversals is shown against a change in potential temperature ( $\Delta\theta$ ) for (a) KF and (b) MDI measurements. Triangles distinguish reversals associated with upwelling-driven AW intrusions. T-S diagrams representing average conditions during the first week of reversals as well as  $\Delta\theta$  at (c) KF and (d) MDI (see color bar). Black labels display dates (month-year) of reversals. Red labels indicate dates of reversals associated to upwelling-driven AW intrusions.

forced by upwelling. This signal reached higher temperatures and arrived 3–4 days earlier in the mid-fjord than the inner-fjord. Furthermore, MDI captured only the most prominent upwelling-driven AW intrusions, whose AW signal reached intermediate depths in the fjord. However, the distinction between years with and without AW intrusions still holds for KF. Indeed, identifying AW intrusions through KF near-bottom temperature and salinity time series reveals the same events with consistent timing as MDI (Figure S5 in Supporting Information S1). Winter 2014 exhibited an intrusion event characterized by a downwelling-driven mechanism, where the warming signal spread from the near-surface to the near-bottom.

#### 4.2. Mechanism of Upwelling-Driven Events

Atmospheric conditions in the first and second week during a wind reversal reflect two different large-scale/synoptic circulations. The strong geopotential dipole characterizing the first week sets up strong geostrophic winds blowing from the south over Fram Strait. Surface waters are moved through Ekman transport toward the physical barrier represented by the West Spitsbergen coast, generating upwelling in the central Fram Strait and strong downwelling on the WSS. The situation changes suddenly in a few days, typically from daily southerlies of 10 m/s to northerlies of 6–7 m/s. The restoration of a low-pressure anomaly triggers northerly winds, initiating upwelling on the WSS, especially on the northern WSS.

Wind reversals over the West Spitsbergen area are the key common factor triggering upwelling-driven events in Kongsfjorden. This dynamic is consistent with the development of the STC on the WSS (Nilsen et al., 2016) and the intermediary circulation between Kongsfjorden and Kongsfjordrenna (Stigebrandt, 1981). Southerly winds and the negative wind stress curl force surface waters to stack up along the West Spitsbergen coast. The resulting increase in the cross-shelf sea surface tilt forces the WSC on shallower isobaths on the shelf, developing the STC.

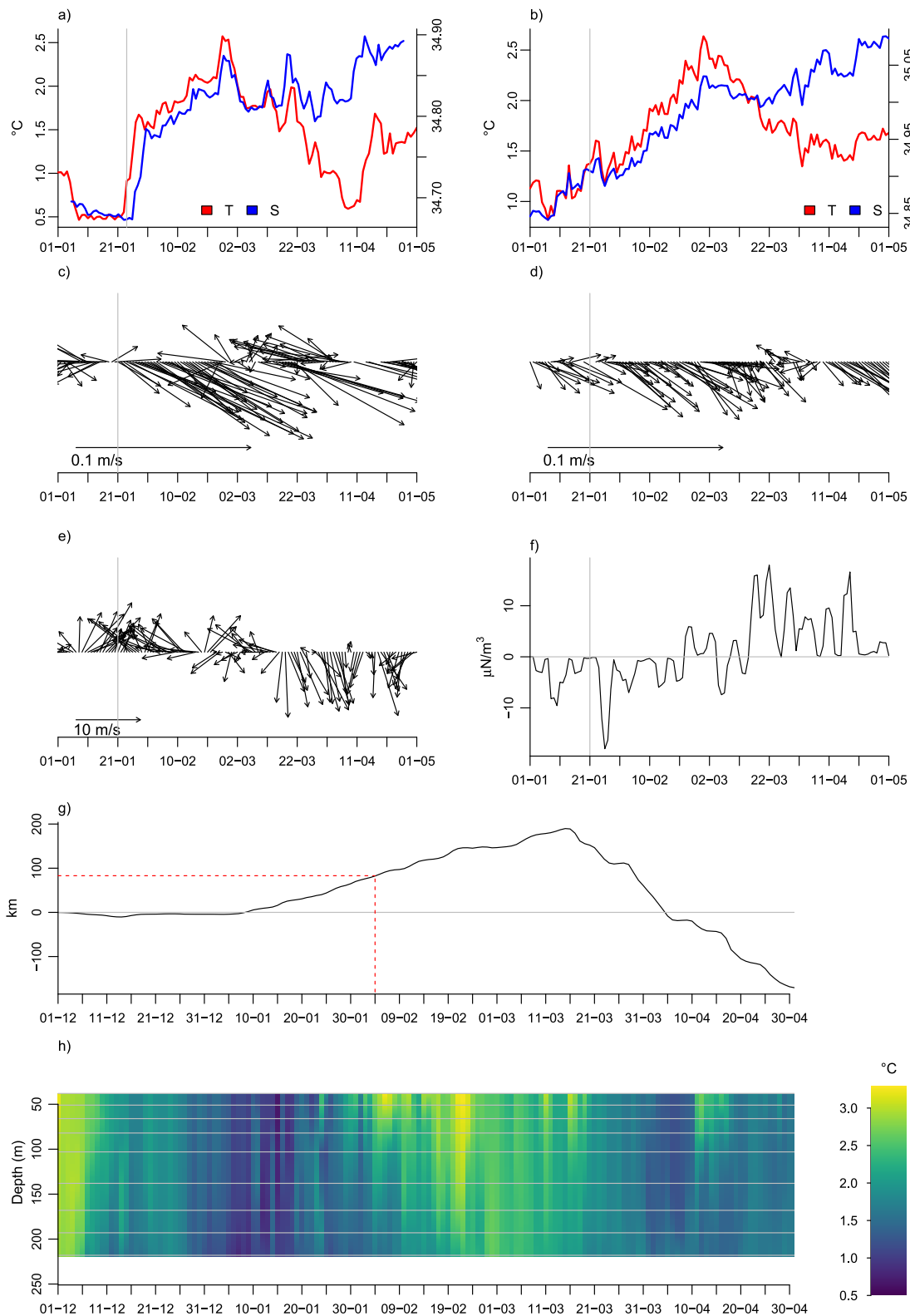


**Figure 6.** Winter 2014 downwelling-driven AW intrusion: temperature and salinity at MDI (a) and KF (b); near-surface (c) and near-bottom (d) currents from KF; average winds (e) and wind stress curl (f) over the shelf (area A1) from ERA5; (g)  $X_{Ek}$  (black line); the horizontal red dashed line highlights the geographical distance between the West Spitsbergen Current (F3 location) and Kongsfjorden (KF location), while the vertical red dashed line highlights the date at which  $X_{Ek}$  reaches this distance (see Section 2.2 for details); (h) KF temperature profile, gray horizontal lines identify sensors' depths. Vertical gray lines represent  $t_0$  dates.

Once southerly winds cease, the sea-surface tilt relaxes, and surface waters tend to flow offshore, compensated by an inflow from the shelf break on the lower levels. AW can now flow toward the fjord at the deepest levels on the shelf. Northerly winds further drive surface waters off Kongsfjorden, compensated by the inflow of AW from the STC near the bottom. AW is uplifted by upwelling and reaches the near surface. Nilsen et al. (2016) found the highest cross-correlations between southerlies and Isfjorden temperature on lags around 50 days. Even though the Kongsfjorden trough is shorter than the Isfjorden trough, KF captures the warming signal just a few days after the outset of southerly winds. This shorter lag may indicate the presence of AW on the shelf already at the time of the *reversal*, the latter generating only fjord-shelf exchanges. Northerly winds upwell fjord deep waters, which are replaced by waters on the shelf, thus disrupting the geostrophic control.

The link of wind *reversals* with the general atmospheric circulation is further examined through a correlation analysis (see Sections 2.1.2 and 2.2 for details). The only significant correlation ( $-0.4$ ,  $p$ -value = 0.01) is found with the Arctic Oscillation (AO). A negative phase of the AO is associated with a weaker jet stream in the northern hemisphere, characterized by large meanders propagating high-pressure anomalies as far north as the Barents Sea and Fram Strait and negative pressure anomalies toward the mid-latitudes. A negative AO phase can thus set up a pressure anomaly field at high latitudes characterized by large zonal gradients, a feature consistent with the geopotential dipole observed in Figure 4a, increasing the probability of large meridional geostrophic winds over the Fram Strait.

*Reversals* occur throughout the year (Figure S6a in Supporting Information S1), and their occurrence peaks in February and October (Figure S6b in Supporting Information S1). *Reversals* occurred almost every winter of the decade, up to three events per season (Figure S6c in Supporting Information S1). Thus, why do upwelling-driven AW intrusions occur only in some winters and do not follow every *reversal* event? *Reversals* are not the only essential aspect determining the characteristics of the AW intrusions, even though they set off the movement of AW toward Kongsfjorden.

The presence of low-density near-bottom waters in the fjord is the critical local oceanic aspect during *reversals* generating upwelling-driven AW intrusions (Figures 5c and 5d). These low-density waters are not confined just to the period preceding the warming, but characterize the whole winter season in years featuring AW intrusions forced by upwelling: 2011, 2016 and 2018 for KF (Figure 7a); 2011, 2012, 2018 and 2020 for MDI (Figure 7b). The low density is linked to a low salinity signal in all these winters, except for 2016 (Figures 7e and 7f). At KF, salinity in 2011 and 2018 dropped right before the beginning of the new year to a local minimum around February (Figure 7e). A similar behavior is observed for MDI (Figure 7f). Here, low salinities characterize January and February of those years with upwelling-driven AW intrusion, that is, 2011, 2012, 2018 and 2020, even though in the inner fjord there is not a clear salinity drop as in the mid-fjord. Winter 2016 features several different AW intrusion events already from the end of 2015 (De Rovere et al., 2022), leaving continuous warm and low-density conditions in the mid-fjord for the whole winter.

The potential density of the AW layer in the WSC exhibits a seasonal pattern, generally increasing from November to May, except for winter 2016 (Figure 8). Fjord density increases over the winter season, but the timing of the inception shows some inter-annual variability, for example, early winter as in 2013, 2014 and 2015, or late winter as in 2011 and 2016. This inter-annual variability in fjord density plays a crucial role in influencing the density difference between incoming WSC waters and fjord waters, ultimately preconditioning the dynamics of AW intrusions.

*Reversals* triggering AW intrusions (indicated by vertical red lines in Figure 8) are associated with AW that is denser than fjord's bottom waters (Figures 8a and 8e). Conversely, when AW is not denser than fjord's bottom water, *reversals* do not trigger upwelling-driven AW intrusions (vertical blue lines in Figure 8). Our interpretation is that denser AW intrudes the fjord beneath lower-density waters. In contrast, when fjord waters have higher or similar densities compared to WSC waters (vertical blue lines in Figure 8), *reversals* generate AW inflows at near-surface or intermediate depths, as in February 2017 (Figure S7 in Supporting Information S1) and March 2015 (Figure S8 in Supporting Information S1), respectively. In such cases, northerly winds may move part of the intruded AW offshore through surface Ekman transport, thus limiting the warming in the fjord. If northerly winds do not follow prolonged southerly winds, then an AW intrusion by downwelling may occur (see Section 4.3 for further details). It is important to note that there are reversals leading to inflowing waters colder than fjord waters, as in February 2015 (Figure S9 in Supporting Information S1), indicating the presence of a cold water mass other than AW on the shelf at the time of these events. Unfortunately, we are not aware of any available measurements

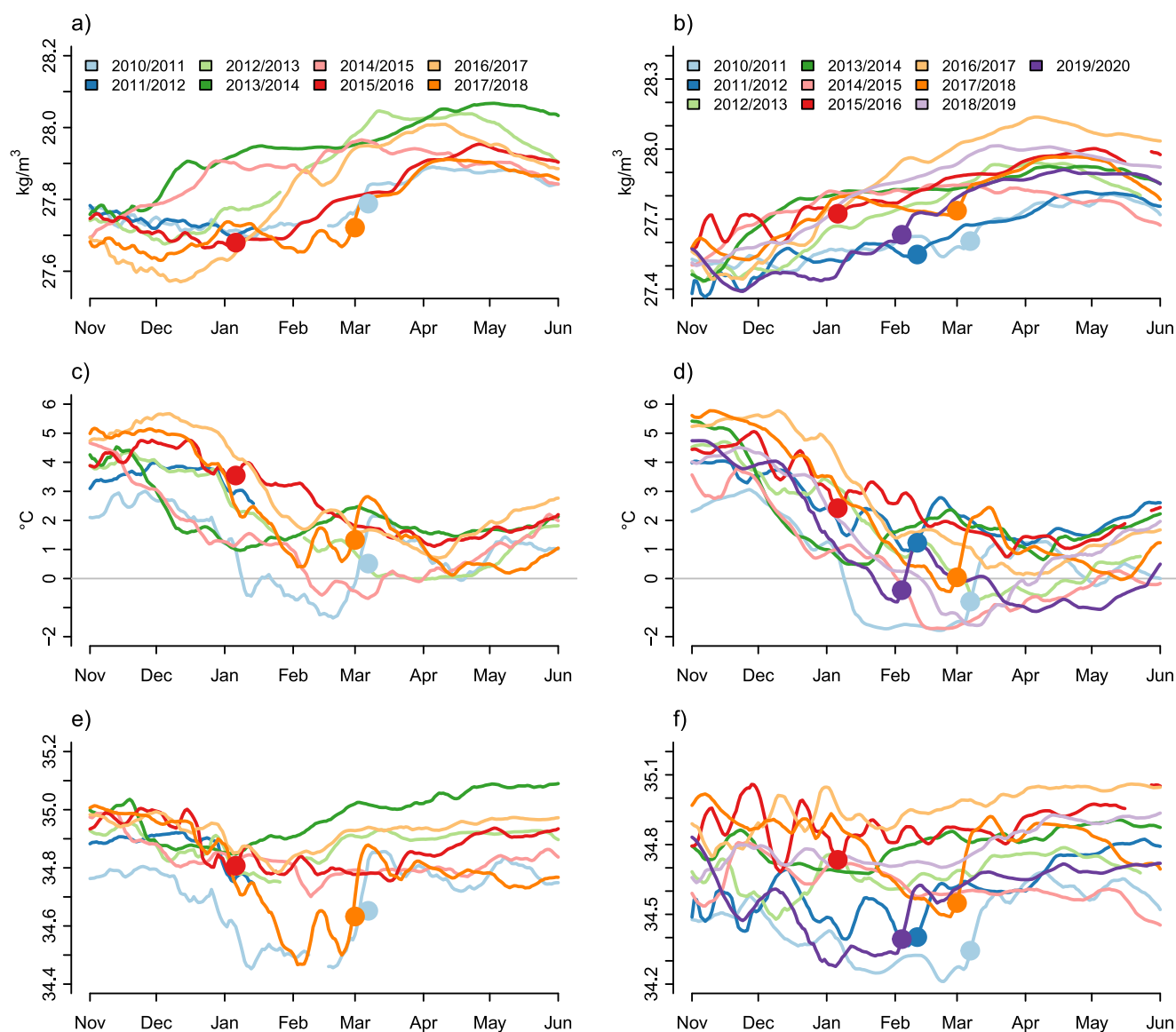


**Figure 7.** Near-bottom potential density (a, b), potential temperature (c, d), and salinity (e, f) at KF (left-side) and MDI (right-side) between November and June. Time series are smoothed with a 7-day moving average. Dots indicate  $t_0$  dates of upwelling-driven AW intrusions at MDI. Note that KF has no measurements for winter 2012, 2019 and 2020.

in Kongsfjordrenna during these events. Such measurements would provide a more comprehensive understanding of the ongoing dynamics and help distinguish water masses present on the shelf.

The occurrence of winter upwelling-driven AW intrusions in Kongsfjorden is principally linked to the fjord's winter density conditions, whose inter-annual variability largely depends on the arrival of fresher waters at the fjord near-bottom (2011, 2012, 2018 and 2020 events). Near-bottom density and salinity from mooring I-S, positioned on the shelf in front of Isfjorden, show an inter-annual variability consistent with KF and MDI data, featuring lower values during winters characterized by upwelling-driven events (Figures S10a and S10c in Supporting Information S1). I-S observations also show that winter 2012, which KF did not record, features a low potential density at the beginning of the season, with values comparable to those of the 2011 and 2018 winters. Hence, low-density waters in years with upwelling-driven AW intrusions are found in both Kongsfjorden and Isfjorden, suggesting a common freshwater source for these two locations. The primary freshwater source in winter in the West Spitsbergen area is the SPC, which transports ArW and sea ice from the Barents Sea through Storfjorden to the WSS, ultimately influencing water masses in Kongsfjorden (Svendsen et al., 2002; Tverberg et al., 2019). The SPC is thus

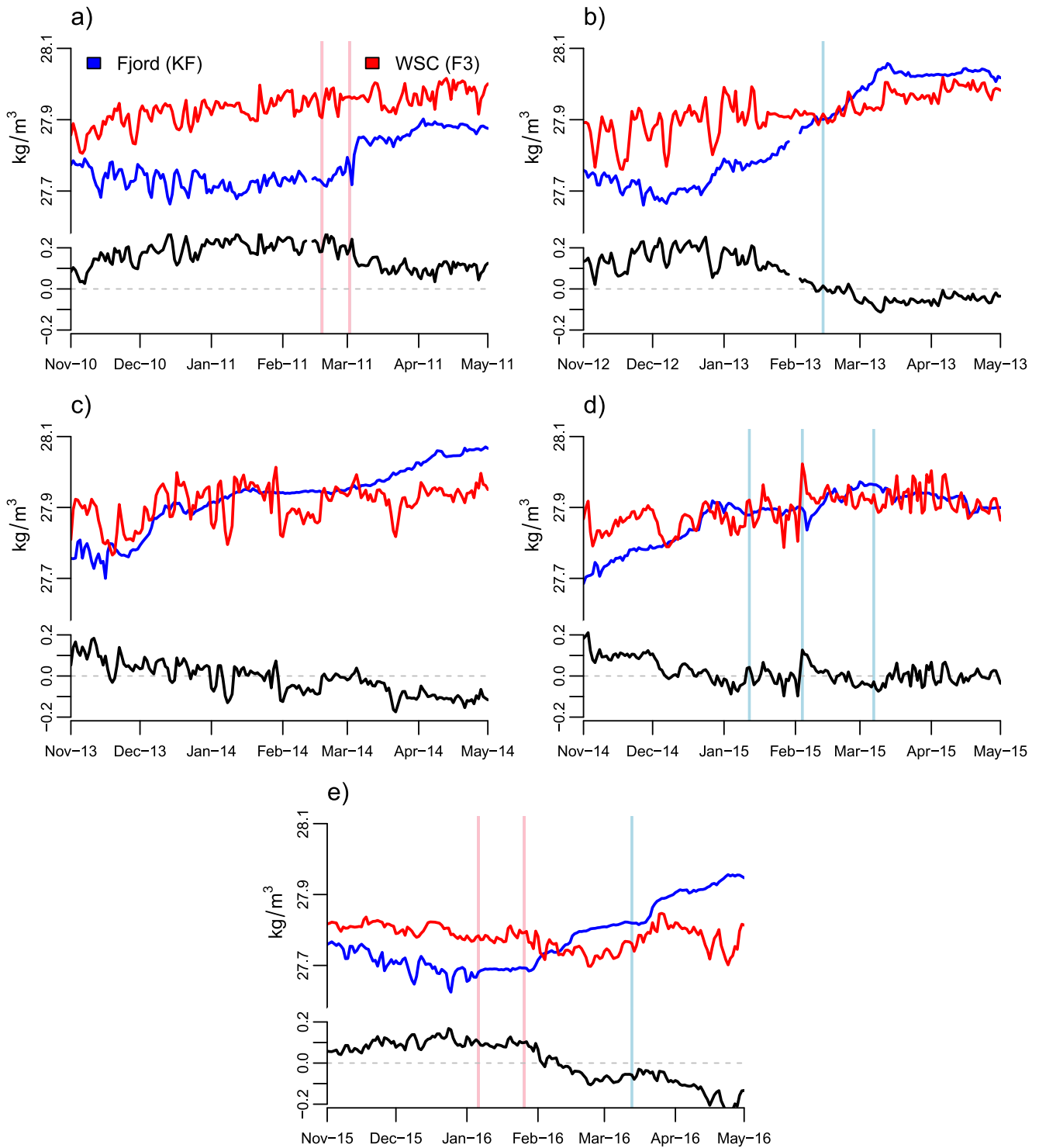


**Figure 8.** (a–e) Potential density at KF (fjord's near-bottom, blue lines) and F3 (intermediate West Spitsbergen Current layer, red lines) between November and May for years with simultaneous measurements. Dates of *reversals* are represented with vertical blue lines, while vertical red lines identify *reversals* associated with AW intrusions (all events are considered and not only the ones leading to the greatest temperature change during a single winter; see methods). Dates of *reversals* are 2013-02-13 (b), 2015-01-12 (d), 2015-02-04 (d), 2015-03-07 (d), 2016-03-13 (e). Dates of *reversals* associated with AW intrusions are 2011-02-18 (a), 2011-03-02 (a), 2016-01-06 (e) and 2016-01-26 (e). The lower side of each subplot reports the difference between F3 and KF potential densities.

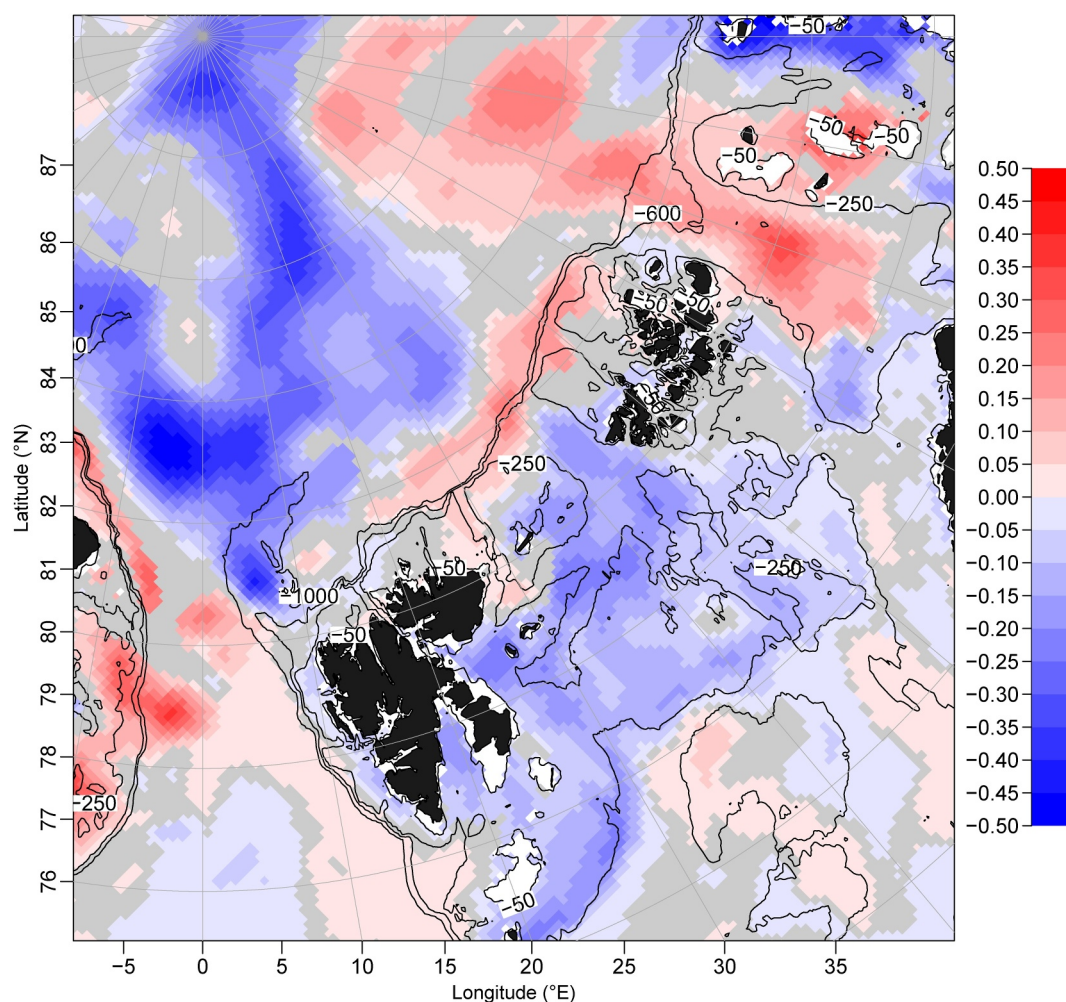


**Figure 9.** January-February mean salinity difference at 50 m depth between winters with and without upwelling-driven AW intrusions as recognised in this study (see Section 2.2 for details). Blue (red) areas are characterized by lower (larger) salinities during years with upwelling-driven AW intrusions in Kongsfjorden. Gray areas identify locations where the salinity difference is not significant. Data come from daily TOPAZ4 reanalyses.

the primary factor preconditioning the inter-annual variability in the shelf and fjords' winter density, eventually determining the characteristics of AW intrusions once triggered by atmospheric *reversals*.

Significantly lower salinities in the WSS at 50 m depth are seen for those years featuring an upwelling-driven AW intrusion (2011, 2012, 2018, 2020) compared to the other winters (2013, 2015, 2017, 2019) (Figure 9). Besides the WSS, this negative salinity anomaly characterizes Storfjorden and the region south of the Svalbard archipelago, the northern Barents Sea and the central Arctic basin. Low-salinity waters in the northern Barents Sea feed the SPC, which redistributes the freshwater signal along the WSS. This large-scale salinity structure might be produced by a significant freshwater export from strong sea ice melting during the previous summer season, a lack of sea ice production in the present autumn/winter and freshwater advection from Siberian rivers. The occurrence of prolonged AW advection in the previous summer/autumn may also leave a denser water column on the WSS and adjacent fjords at the end of the year, conditioning the winter density as well. Future research efforts should focus on understanding the causes of such large inter-annual variability in the density of the WSS and adjacent fjords.

### 4.3. The Downwelling Mechanism

The winter 2014 AW intrusion showed an initial warming in the upper layer of the water column, which then propagated toward the bottom, likely due to heat loss and densification. We hypothesize that long-lasting,



constant southerly winds transported the shallowest WSC layers toward the fjord, which were eventually forced to enter on top of fjord waters. The timing in which the theoretical Ekman layer arrives in the fjord supports this hypothesis (Figure 6g), which is concurrent with the arrival of warm waters near the surface (Figures 6a–6i). A significant difference with the upwelling mechanism described in Section 4.2 is the absence of sustained northerly winds, which could have limited the fjord's warming by moving the near-surface AW offshore through Ekman transport. Furthermore, winter 2014 is the second warmest winter at the near surface (70 m depth), as well as the winter with the highest temperature difference between 70 and 250 m depth, according to 13 years of F3 measurements from 1999 to 2015 (Figure S11 in Supporting Information S1). This evidence indicates that the core of the WSC was shallower in winter 2014 than in other years, and southerly winds could have easily transported warm waters toward the coast of Spitsbergen through Ekman transport.

Winter 2014 is characterized by a strong positive geopotential height anomaly centered over the Barents Sea, developing in January (Figure 10b) and persisting until February (Figure 10c), while a strong negative geopotential anomaly develops in the northeastern Atlantic region, between Iceland and Great Britain. Consequently, winter 2014 features a continuously rising cumulative meridional wind stress, reaching the largest cumulative values of the decade (Figure 10e). This particular atmospheric setting generates southerly winds over the Fram Strait persistently for 2 months.

#### 4.4. Relation With Winter Scenarios

The different AW intrusion mechanisms proposed in this study are linked to the Winter Scenarios introduced by Tverberg et al. (2019), describing the character of the wintertime AW intrusion in Kongsfjorden (see Section 1). The upwelling mechanism fits the *Winter Intermediate* scenario, where the AW intrusion occurs at depth and, depending on the magnitude of the upwelling, it can reach the fjord surface. The downwelling mechanism fits the *Winter Open* scenario, where the AW is forced eastward by persistent southerly winds and intrudes on top of fjord waters. Winters characterized by the absence of substantial AW inflows are consistent with the *Winter Deep* scenario, where the fjord's water column undergoes convection and densification. In the case of *Winter Open* and *Deep*, large fjord densities could also be related to the occurrence of extensive AW intrusion in the previous autumn season, which leaves a denser water column for the subsequent winter.

### 5. Summary and Conclusions

Wintertime AW intrusions in Kongsfjorden are relatively common events in the 2011–2020 decade. These events lead to a temperature, salinity and density increase in the fjord of at least 1°C, 0.1 and 0.03 kg/m<sup>3</sup>, respectively, in just a few days, leaving a warmer and denser water column lasting for a few weeks after their occurrence. Five major events took place in winter 2011, 2012, 2016, 2018 and 2020 by means of upwelling. AW intrusions are triggered by energetic wind *reversals* blowing over the WSS, consisting of strong southerly winds leading to downwelling conditions, followed by northerly winds and upwelling conditions. *Reversals* activate intermediary circulation and move WSC waters on the shallower isobaths on the WSS, setting up the STC transporting AW toward Kongsfjorden. Southerlies are developed by the setup of a strong pressure dipole, with a high-pressure center over the Barents Sea and a low-pressure center over Greenland and Northern Canada. Afterward, the restoration of the typical low-pressure conditions over the Central Arctic and the Svalbard archipelago generates northerly winds. The occurrence of wind *reversals* is significantly anti-correlated with the AO, as a negative AO phase is more likely to trigger the pressure dipole associated with such wind events.

The ocean is a crucial preconditioning factor, limiting upwelling-driven AW intrusions only to those periods when fjord waters are less dense than WSC waters. External advection of fresher (2011, 2012, 2018 and 2020 events) or warmer (2016 event) waters before the intrusion lowers the fjord's bottom density. The SPC is the key driver of the freshwater input, which transports anomalously low salinity waters from the northern Barents Sea to the WSS. In contrast, when fjord waters have higher or similar densities compared to WSC waters, *reversals* generate AW inflows at near-surface or intermediate depths. The 2014 intrusion event occurred by means of downwelling. On the WSS, southerly winds blew almost persistently during January and February, transporting AW from the top layers of the WSC toward Kongsfjorden, which then intruded on top of fjord waters. Southerly winds were generated by a long-lasting high-pressure anomaly over the Barents Sea and the Eurasian Arctic region, which contrasted with a low-pressure anomaly over the northeastern Atlantic Ocean.

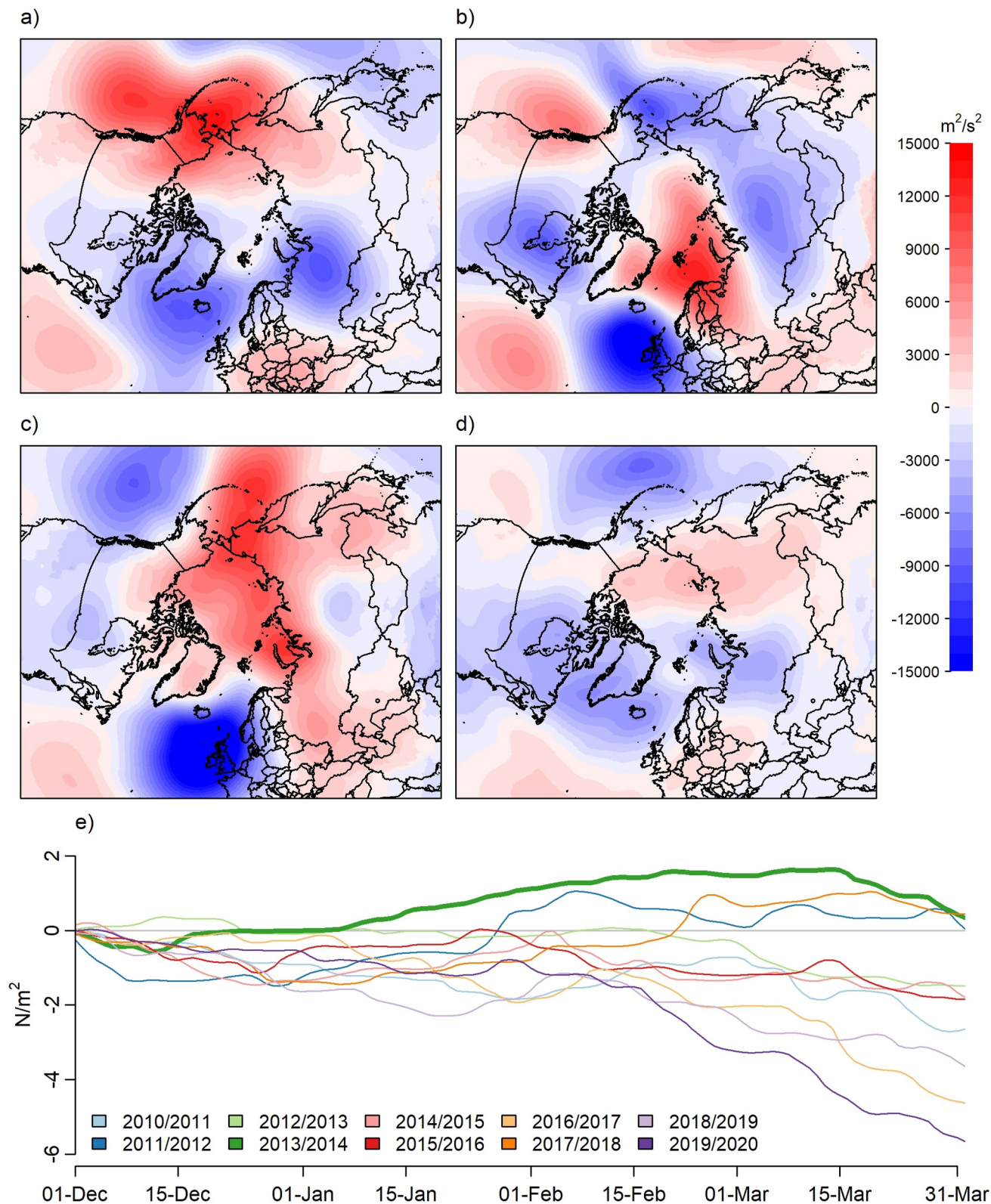


**Figure 10.** Atmospheric conditions in winter 2014. Anomaly of mean geopotential height at 850 hPa in December 2013 (a), January 2014 (b), February 2014 (c) and March 2014 (d). Climatology is computed over the 2011–2020 decade. (e) Cumulative meridional wind stress from December to April for winters in the 2011–2020 decade. The thick green line highlights winter 2014.

This study improved the understanding of winter AW intrusion mechanisms by discussing the dynamical aspects of several observed events. The emerging picture shows that both the atmospheric and oceanic components are relevant in determining the timing and characteristics of the intrusions and, more generally, of Kongsfjorden's winter conditions. Furthermore, the SPC plays a critical role by transporting the low-density signal from the northern Barents Sea over the WSS to the adjacent fjords, which allows for the development of upwelling-driven AW intrusions.

## Data Availability Statement

MDI and CCT data (CNR – National Research Council of Italy, 2022) are stored in the Italian Arctic Data Center at [https://data.iadc.cnr.it/erddap/files/mdi\\_ctd\\_timeseries\\_1/](https://data.iadc.cnr.it/erddap/files/mdi_ctd_timeseries_1/). KF temperature and salinity data (Cottier et al., 2021a, 2021b, 2021c, 2022a, 2022b, 2022c, 2022d, 2022e, 2022f, 2022g, 2022h, 2022i), as well as ADCP raw data (Cottier et al., 2023a, Cottier et al., 2021c, 2023c, 2023d, 2023e) are available in the NIRD research data archive ([archive.sigma2.no](https://archive.sigma2.no)). F3 data (Beszczynska-Möller, Fahrbach, Rohardt, & Schauer, 2012; Beszczynska-Möller et al., 2015; von Appen et al., 2015, 2017) can be found in the PANGAEA data archive ([doi.pangaea.de/10.1594/PANGAEA.900883](https://doi.pangaea.de/10.1594/PANGAEA.900883)). I-S data (Skogseth & Ellingsen, 2019a, 2019b, 2019c, 2019d, 2019e, 2019f, 2019g, 2019h) can be found at the Norwegian Polar Data Centre ([data.npolar.no/home/](https://data.npolar.no/home/)). ERA5 hourly data on single levels (Hersbach et al., 2023b) are available at [doi.org/10.24381/cds.adbb2d47](https://doi.org/10.24381/cds.adbb2d47). ERA5 hourly data (Hersbach et al., 2023a) and monthly averaged data (Hersbach et al., 2023c) on pressure levels are available at [doi.org/10.24381/cds.bd0915c6](https://doi.org/10.24381/cds.bd0915c6) and [doi.org/10.24381/cds.6860a573](https://doi.org/10.24381/cds.6860a573), respectively. CMEMS Arctic Ocean Physics Reanalysis data from the E.U. Copernicus Marine Service Information (CMEMS – Copernicus Marine Service, 2022) are accessible at [doi.org/10.48670/moi-00007](https://doi.org/10.48670/moi-00007). The time series of NOAA CPC northern hemisphere teleconnection patterns (NOAA, 2012) can be retrieved from [ftp://ftp.cpc.ncep.noaa.gov/wd52dg/data/indices/tele\\_index.nh](https://ftp.cpc.ncep.noaa.gov/wd52dg/data/indices/tele_index.nh).

## Acknowledgments

We thank the two anonymous reviewers for their insightful comments and constructive feedback, which significantly contributed to the improvement of this manuscript. We acknowledge the financial support by the Programma di Ricerche in Artico (PRA) through the PhD fellowship awarded to FDR. We would like to thank the CNR Arctic Station Dirigibile Italia and Kings Bay AS for logistic support. ADCP and CTD data for mooring KF were provided by the Kongsfjorden Rijpfjorden Observatory Program (KROP), which has been supported by the UK Natural Environment Research Council (Oceans 2025 and Northern Sea Program) and the Research Council of Norway (projects Cleopatra: 178766, Cleopatra II: 216537, Circa: 214271/F20, Marine Night: 26471, FAABulous: 243702, ArcticABC: 244319 and Deep Impact: 300333). We would like to acknowledge the UNIS courses AB-320 and AB-321 for the cooperation in the use of ship time. We thank Daniel Ludwig Vogedes for sharing KF's ADCP data.

## References

- Barnston, A. G., & Livezey, R. E. (1987). Classification, seasonality and persistence of low-frequency atmospheric circulation patterns. *Monthly Weather Review*, 115(6), 1083–1126. [https://doi.org/10.1175/1520-0493\(1987\)115<1083:csapol>2.0.co;2](https://doi.org/10.1175/1520-0493(1987)115<1083:csapol>2.0.co;2)
- Beszczynska-Möller, A., Fahrbach, E., Schauer, U., & Hansen, E. (2012). Variability in Atlantic water temperature and transport at the entrance to the Arctic Ocean, 1997–2010. *ICES Journal of Marine Science*, 69(5), 852–863. <https://doi.org/10.1093/icesjms/fss056>
- Beszczynska-Möller, A., Fahrbach, E., Rohardt, G., & Schauer, U. (2012). Physical oceanography and current meter data from mooring F3-13 [Dataset]. PANGAEA. <https://doi.org/10.1594/PANGAEA.800342>
- Beszczynska-Möller, A., von Appen, W.-J., & Fahrbach, E. (2015). Physical oceanography and current meter data from mooring F3-14 [Dataset]. PANGAEA. <https://doi.org/10.1594/PANGAEA.845648>
- Bischof, K., Convey, P., Duarte, P., Gattuso, J. P., Granberg, M., Hop, H., et al. (2019). *Kongsfjorden as harbinger of the future Arctic: Knowns, unknowns and research priorities* (pp. 537–562). The ecosystem of Kongsfjorden, Svalbard.
- Bloshkina, E. V., Pavlov, A. K., & Filchuk, K. (2021). Warming of Atlantic water in three West Spitsbergen fjords: Recent patterns and century-long trends. *Polar Research*, 40. <https://doi.org/10.33265/polar.v40.5392>
- Carmack, E., Polyakov, I., Padman, L., Fer, I., Hunke, E., Hutchings, J., et al. (2015). Toward quantifying the increasing role of oceanic heat in sea ice loss in the new Arctic. *Bulletin of the American Meteorological Society*, 96(12), 2079–2105. <https://doi.org/10.1175/bams-d-13-00177.1>
- Chatterjee, S., Raj, R. P., Bertino, L., Skagseth, Ø., Ravichandran, M., & Johannessen, O. M. (2018). Role of Greenland Sea gyre circulation on Atlantic water temperature variability in the Fram Strait. *Geophysical Research Letters*, 45(16), 8399–8406. <https://doi.org/10.1029/2018gl079174>
- Chree, C. (1912). Some phenomena of sunspots and of terrestrial magnetism, at Kew observatory. *Philosophical Transactions of the Royal Society of London, Series A*, 212, 75.
- Chree, C. (1913). Some phenomena of sunspots and of terrestrial magnetism, II. *Philosophical Transactions of the Royal Society of London, Series A*, 213, 245.
- Chylek, P., Folland, C. K., Lesins, G., Dubey, M. K., & Wang, M. (2009). Arctic air temperature change amplification and the Atlantic Multidecadal Oscillation. *Geophysical Research Letters*, 36(14). <https://doi.org/10.1029/2009gl038777>
- CMEMS – Copernicus Marine Service. (2022). Arctic Ocean Physics reanalysis [Dataset]. *Copernicus Marine Data Store*. <https://doi.org/10.48670/moi-00007>
- CNR – National Research Council of Italy. (2022). CTD data set from mooring MDI @ 35m and 85m (Kongsfjorden) [Dataset]. *Italian Arctic Data Center*. [https://data.iadc.cnr.it/erddap/info/mdi\\_ctd\\_timeseries\\_1/index.html](https://data.iadc.cnr.it/erddap/info/mdi_ctd_timeseries_1/index.html)
- Comiso, J. C. (2012). Large decadal decline of the Arctic multiyear ice cover. *Journal of Climate*, 25(4), 1176–1193. <https://doi.org/10.1175/jcli-d-11-00113.1>
- Cottier, F., Berge, J., Dumont, E., Griffith, C., Beaton, J., & UiT The Arctic University of Norway, Scottish Association for Marine Science. (2021b). Temperature, salinity, light and fluorescence (CTD) measurements from the Kongsfjorden (Svalbard) marine observatory (mooring) August 2016–August 2017 [Dataset]. *Norstore*. <https://doi.org/10.11582/2021.00062>
- Cottier, F., Berge, J., Dumont, E., Kopec, T. P., Venables, E. J., Vogedes, D. L., & UiT The Arctic University of Norway, Scottish Association for Marine Science. (2021c). Temperature, salinity, light and fluorescence (CTD) measurements from the Kongsfjorden (Svalbard) marine observatory (mooring) August 2017–August 2018 [Dataset]. *Norstore*. <https://doi.org/10.11582/2021.00065>

- Cottier, F., Berge, J., Dumont, E., Kopec, T. P., Venables, E. J., & Vogedes, D. L., & UiT The Arctic University of Norway, Scottish Association for Marine Science. (2023a). ADCP measurements from the Kongsfjorden (Svalbard) marine observatory (mooring) August 2017-August 2018 [Dataset]. *Norstore*. <https://doi.org/10.11582/2023.00060>
- Cottier, F., Berge, J., Griffith, C., Dumont, E., Beaton, J., & Vogedes, D. L., & UiT The Arctic University of Norway, Scottish Association for Marine Science. (2021a). Temperature, salinity, light and fluorescence (CTD) measurements from the Kongsfjorden (Svalbard) marine observatory (mooring) September 2015-August 2016 [Dataset]. *Norstore*. <https://doi.org/10.11582/2021.00061>
- Cottier, F., Berge, J., Griffith, C., Dumont, E., Beaton, J., & Vogedes, D. L., & UiT The Arctic University of Norway, Scottish Association for Marine Science. (2022h). Temperature, salinity, light and fluorescence (CTD) measurements from the Kongsfjorden (Svalbard) marine observatory (mooring) September 2013-October 2014 [Dataset]. *Norstore*. <https://doi.org/10.11582/2022.00018>
- Cottier, F., Berge, J., Griffith, C., Dumont, E., Beaton, J., & Vogedes, D. L., & UiT The Arctic University of Norway, Scottish Association for Marine Science. (2023b). ADCP measurements from the Kongsfjorden (Svalbard) marine observatory (mooring) September 2015- September 2016 [Dataset]. *Norstore*. <https://doi.org/10.11582/2023.00058>
- Cottier, F., Berge, J., Griffith, C., Dumont, E., Beaton, J., Vogedes, D. L., et al. UiT The Arctic University of Norway, Scottish Association for Marine Science. (2022i). Temperature, salinity, light and fluorescence (CTD) measurements from the Kongsfjorden (Svalbard) marine observatory (mooring) September 2014-September 2015 [Dataset]. *Norstore*. <https://doi.org/10.11582/2022.00019>
- Cottier, F., Berge, J., Griffith, C., Dumont, E., Kopec, T. P., & Vogedes, D. L., & UiT The Arctic University of Norway, Scottish Association for Marine Science. (2022a). Temperature, salinity and fluorescence (CTD) measurements from the Kongsfjorden (Svalbard) marine observatory (mooring) June 2006-August 2007 [Dataset]. *Norstore*. <https://doi.org/10.11582/2022.00024>
- Cottier, F., Berge, J., Griffith, C., Dumont, E., Kopec, T. P., & Vogedes, D. L., & UiT The Arctic University of Norway, Scottish Association for Marine Science. (2022b). Temperature, salinity, light and fluorescence (CTD) measurements from the Kongsfjorden (Svalbard) marine observatory (mooring) August 2007-August 2008 [Dataset]. *Norstore*. <https://doi.org/10.11582/2022.00025>
- Cottier, F., Berge, J., Griffith, C., Dumont, E., Kopec, T. P., & Vogedes, D. L., & UiT The Arctic University of Norway, Scottish Association for Marine Science. (2022c). Temperature, salinity, light and fluorescence (CTD) measurements from the Kongsfjorden (Svalbard) marine observatory (mooring) September 2008-August 2009 [Dataset]. *Norstore*. <https://doi.org/10.11582/2022.00026>
- Cottier, F., Berge, J., Griffith, C., Dumont, E., Kopec, T. P., & Vogedes, D. L., & UiT The Arctic University of Norway, Scottish Association for Marine Science. (2022d). Temperature, salinity, light and fluorescence (CTD) measurements from the Kongsfjorden (Svalbard) marine observatory (mooring) September 2009-September 2010 [Dataset]. *Norstore*. <https://doi.org/10.11582/2022.00022>
- Cottier, F., Berge, J., Griffith, C., Dumont, E., Kopec, T. P., & Vogedes, D. L. (2022f). Temperature, salinity, light and fluorescence (CTD) measurements from the Kongsfjorden (Svalbard) marine observatory (mooring) September 2011-September 2012 [Dataset]. *Norstore*. <https://doi.org/10.11582/2022.00020>
- Cottier, F., Berge, J., Griffith, C., Dumont, E., Kopec, T. P., & Vogedes, D. L., & UiT The Arctic University of Norway, Scottish Association for Marine Science. (2022g). Temperature, salinity, light and fluorescence (CTD) measurements from the Kongsfjorden (Svalbard) marine observatory (mooring) October 2012-September 2013 [Dataset]. *Norstore*. <https://doi.org/10.11582/2022.00021>
- Cottier, F., Berge, J., Griffith, C., Dumont, E., Kopec, T. P., & Vogedes, D. L., & UiT The Arctic University of Norway, Scottish Association for Marine Science. (2023c). ADCP measurements from the Kongsfjorden (Svalbard) marine observatory (mooring) October 2013-September 2014 [Dataset]. *Norstore*. <https://doi.org/10.11582/2023.00055>
- Cottier, F., Griffith, C., Dumont, E., Kopec, T. P., & Vogedes, D. L., & UiT The Arctic University of Norway, Scottish Association for Marine Science. (2022e). Temperature, salinity, light and fluorescence (CTD) measurements from the Kongsfjorden (Svalbard) marine observatory (mooring) September 2010-September 2011 [Dataset]. *Norstore*. <https://doi.org/10.11582/2022.00023>
- Cottier, F., Griffith, C., Dumont, E., Kopec, T. P., & Vogedes, D. L., & UiT The Arctic University of Norway, Scottish Association for Marine Science. (2023d). ADCP measurements from the Kongsfjorden (Svalbard) marine observatory (mooring) September 2011- September 2012 [Dataset]. *Norstore*. <https://doi.org/10.11582/2023.00052>
- Cottier, F., Griffith, C., Dumont, E., Kopec, T. P., & Vogedes, D. L., & UiT The Arctic University of Norway, Scottish Association for Marine Science. (2023e). ADCP measurements from the Kongsfjorden (Svalbard) marine observatory (mooring) September 2010-September 2011 [Dataset]. *Norstore*. <https://doi.org/10.11582/2023.00051>
- Cottier, F., Skogseth, R., David, D., & Berge, J. (2019). Temperature time-series in Svalbard fjords. A contribution from the “Integrated marine observatory Partnership (iMOP)”. In E. Orr, G. Hansen, H. Lappalainen, C. Hübner, & H. Lihavainen (Eds.), *The e State of Environmental Science in Svalbard report 2018* (pp. 108–118). Longyearbyen: Svalbard Integrated Arctic Earth Observing System.
- Cottier, F., Tverberg, V., Inall, M., Svendsen, H., Nilsen, F., & Griffiths, C. (2005). Water mass modification in an Arctic fjord through cross-shelf exchange: The seasonal hydrography of Kongsfjorden, Svalbard. *Journal of Geophysical Research*, *110*(C12). <https://doi.org/10.1029/2004jc002757>
- Cottier, F. R., Nilsen, F., Inall, M. E., Gerland, S., Tverberg, V., & Svendsen, H. (2007). Wintertime warming of an Arctic shelf in response to large-scale atmospheric circulation. *Geophysical Research Letters*, *34*(10). <https://doi.org/10.1029/2007gl029948>
- Curry, J. A., Schramm, J. L., & Ebert, E. E. (1995). Sea ice-albedo climate feedback mechanism. *Journal of Climate*, *8*(2), 240–247. [https://doi.org/10.1175/1520-0442\(1995\)008<0240:siacfm>2.0.co;2](https://doi.org/10.1175/1520-0442(1995)008<0240:siacfm>2.0.co;2)
- Cushman-Roisin, B., & Beckers, J. M. (2011). *Introduction to geophysical fluid dynamics: Physical and numerical aspects*. Academic Press.
- D'Angelo, A., Giglio, F., Miserocchi, S., Sanchez-Vidal, A., Aliani, S., Tesi, T., et al. (2018). Multi-year particle fluxes in Kongsfjorden, Svalbard. *Biogeosciences*, *15*(17), 5343–5363. <https://doi.org/10.5194/bg-15-5343-2018>
- De Rovere, F., Langone, L., Schroeder, K., Miserocchi, S., Giglio, F., Aliani, S., & Chiggiato, J. (2022). Water masses variability in inner Kongsfjorden (Svalbard) during 2010–2020. *Frontiers in Marine Science*, *9*. <https://doi.org/10.3389/fmars.2022.741075>
- Foreman, M. G. G. (1978). Manual for tidal currents analysis and prediction, Pacific marine science report 78-6. Institute of Ocean Sciences, Patricia Bay, Sidney. British Columbia, 70.
- Goszczko, I., Ingvaldsen, R. B., & Onarheim, I. H. (2018). Wind-driven cross-shelf exchange—West Spitsbergen current as a source of heat and salt for the adjacent shelf in Arctic winters. *Journal of Geophysical Research: Oceans*, *123*(4), 2668–2696. <https://doi.org/10.1002/2017jc013553>
- Häkkinen, S., Rhines, P. B., & Worthen, D. L. (2011). Atmospheric blocking and Atlantic multidecadal ocean variability. *Science*, *334*(6056), 655–659. <https://doi.org/10.1126/science.1205683>
- Hegseth, E. N., & Tverberg, V. (2013). Effect of Atlantic water inflow on timing of the phytoplankton spring bloom in a high Arctic fjord (Kongsfjorden, Svalbard). *Journal of Marine Systems*, *113*, 94–105. <https://doi.org/10.1016/j.jmarsys.2013.01.003>
- Helland-Hansen, B., & Nansen, F. (1909). Die jährlichen Schwankungen der Wassermassen im norwegischen Nordmeer in ihrer Beziehung zu den Schwankungen der meteorologischen Verhältnisse, der Ernteerträge und der Fischereiergebnisse in Norwegen. *Internationale Revue der gesamten Hydrobiologie und Hydrographie*, *2*(3), 337–361. <https://doi.org/10.1002/iroh.19090020302>

- Hersbach, H., Bell, B., Berrisford, P., Biavati, G., Horányi, A., Muñoz Sabater, J., et al. (2023a). ERA5 hourly data on pressure levels from 1940 to present [Dataset]. *Copernicus Climate Change Service (C3S) Climate Data Store (CDS)*. <https://doi.org/10.24381/cds.bd0915c6>
- Hersbach, H., Bell, B., Berrisford, P., Biavati, G., Horányi, A., Muñoz Sabater, J., et al. (2023b). ERA5 hourly data on single levels from 1940 to present [Dataset]. *Copernicus Climate Change Service (C3S) Climate Data Store (CDS)*. <https://doi.org/10.24381/cds.adbb2d47>
- Hersbach, H., Bell, B., Berrisford, P., Biavati, G., Horányi, A., Muñoz Sabater, J., et al. (2023c). ERA5 monthly averaged data on pressure levels from 1940 to present [Dataset]. *Copernicus Climate Change Service (C3S) Climate Data Store (CDS)*. <https://doi.org/10.24381/cds.6860a573>
- Holmes, F. A., Kirchner, N., Kuttenukeuler, J., Krützfeldt, J., & Noormets, R. (2019). Relating ocean temperatures to frontal ablation rates at Svalbard tidewater glaciers: Insights from glacier proximal datasets. *Scientific Reports*, 9(1), 1–11. <https://doi.org/10.1038/s41598-019-45077-3>
- Hop, H., & Wiencke, C. (2019). *The ecosystem of Kongsfjorden, Svalbard* (pp. 1–20). Springer International Publishing.
- Inall, M. E., Nilsen, F., Cottier, F. R., & Daae, R. (2015). Shelf/fjord exchange driven by coastal-trapped waves in the Arctic. *Journal of Geophysical Research: Oceans*, 120(12), 8283–8303. <https://doi.org/10.1002/2015jc011277>
- Ingvaldsen, R. B., Assmann, K. M., Primicerio, R., Fossheim, M., Polyakov, I. V., & Dolgov, A. V. (2021). Physical manifestations and ecological implications of Arctic Atlantification. *Nature Reviews Earth & Environment*, 2(12), 874–889. <https://doi.org/10.1038/s43017-021-00228-x>
- Jackson, R. H., Straneo, F., & Sutherland, D. A. (2014). Externally forced fluctuations in ocean temperature at Greenland glaciers in non-summer months. *Nature Geoscience*, 7(7), 503–508. <https://doi.org/10.1038/ngeo2186>
- Kelley, D., & Richards, C. (2022). oce: Analysis of Oceanographic Data [Software]. R package version 1.8-3. <https://CRAN.R-project.org/package=oce>
- Klinck, J. M., O'Brien, J. J., & Svendsen, H. (1981). A simple model of fjord and coastal circulation interaction. *Journal of Physical Oceanography*, 11(12), 1612–1626. [https://doi.org/10.1175/1520-0485\(1981\)011<1612:asmofa>2.0.co;2](https://doi.org/10.1175/1520-0485(1981)011<1612:asmofa>2.0.co;2)
- Lind, S., Ingvaldsen, R. B., & Furevik, T. (2018). Arctic warming hotspot in the northern Barents Sea linked to declining sea-ice import. *Nature Climate Change*, 8(7), 634–639. <https://doi.org/10.1038/s41558-018-0205-y>
- Luckman, A., Benn, D. I., Cottier, F., Bevan, S., Nilsen, F., & Inall, M. (2015). Calving rates at tidewater glaciers vary strongly with ocean temperature. *Nature Communications*, 6(1), 1–7. <https://doi.org/10.1038/ncomms9566>
- Mazzola, M., Viola, A. P., Lanconelli, C., & Vitale, V. (2016). Atmospheric observations at the Amundsen-Nobile climate change tower in Ny-Ålesund, Svalbard. *Rendiconti Lincei*, 27(S1), 7–18. <https://doi.org/10.1007/s12210-016-0540-8>
- Meredith, M., Sommerkorn, M., Cassotta, S., Derksen, C., Ekaykin, A., Hollowed, A., et al. (2019). Polar regions. In H.-O. Pörtner, D. C. Roberts, V. Masson-Delmotte, P. Zhai, M. Tignor, E. Poloczanska, et al. (Eds.), *IPCC special report on the ocean and cryosphere in a changing climate* (pp. 203–320). Cambridge University Press. <https://doi.org/10.1017/9781009157964.005>
- Muiliwijk, M., Smedsrud, L. H., Ilicak, M., & Drange, H. (2018). Atlantic Water heat transport variability in the 20th century Arctic Ocean from a global ocean model and observations. *Journal of Geophysical Research: Oceans*, 123(11), 8159–8179. <https://doi.org/10.1029/2018jc014327>
- Nilsen, F., Gjevik, B., & Schauer, U. (2006). Cooling of the West Spitsbergen current: Isopycnal diffusion by topographic vorticity waves. *Journal of Geophysical Research*, 111(C8). <https://doi.org/10.1029/2005jc002991>
- Nilsen, F., Skogseth, R., Vaardal-Lunde, J., & Inall, M. (2016). A simple shelf circulation model: Intrusion of Atlantic water on the West Spitsbergen shelf. *Journal of Physical Oceanography*, 46(4), 1209–1230. <https://doi.org/10.1175/jpo-d-15-0058.1>
- NOAA (National Oceanic and Atmospheric Administration). (2012). Northern hemisphere teleconnection patterns [Dataset]. <https://www.cpc.ncep.noaa.gov/data/teledoc/telecontents.shtml>
- Payne, C. M., & Roesler, C. S. (2019). Characterizing the influence of Atlantic water intrusion on water mass formation and phytoplankton distribution in Kongsfjorden, Svalbard. *Continental Shelf Research*, 191, 104005. <https://doi.org/10.1016/j.csr.2019.104005>
- Polyakov, I. V., Pnyushkov, A. V., Alkire, M. B., Ashik, I. M., Baumann, T. M., Carmack, E. C., et al. (2017). Greater role for Atlantic inflows on sea-ice loss in the Eurasian basin of the Arctic Ocean. *Science*, 356(6335), 285–291. <https://doi.org/10.1126/science.aai8204>
- Raj, R. P., Nilsen, J. Ø., Johannessen, J. A., Furevik, T., Andersen, O. B., & Bertino, L. (2018). Quantifying Atlantic water transport to the Nordic seas by remote sensing. *Remote Sensing of Environment*, 216, 758–769. <https://doi.org/10.1016/j.rse.2018.04.055>
- Richter-Menge, J., & Druckenmiller, M. L. (2020). State of the climate in 2019. *Arctic*, 101(8), S239–S286.
- Rogers, J. C., Yang, L., & Li, L. (2005). The role of Fram Strait winter cyclones on sea ice flux and on Spitsbergen air temperatures. *Geophysical Research Letters*, 32(6). <https://doi.org/10.1029/2004gl022262>
- Ruggieri, P., Alvarez-Castro, M. C., Athanasiadis, P., Bellucci, A., Materia, S., & Gualdi, S. (2020). North Atlantic circulation regimes and heat transport by synoptic eddies. *Journal of Climate*, 33(11), 4769–4785. <https://doi.org/10.1175/jcli-d-19-0498.1>
- Sakov, P., Counillon, F., Bertino, L., Liseter, K. A., Oke, P. R., & Korabev, A. (2012). TOPAZ4: An ocean-sea ice data assimilation system for the North Atlantic and Arctic. *Ocean Science*, 8(4), 633–656. <https://doi.org/10.5194/os-8-633-2012>
- Serreze, M. C., & Barry, R. G. (2011). Processes and impacts of Arctic amplification: A research synthesis. *Global and Planetary Change*, 77(1–2), 85–96. <https://doi.org/10.1016/j.gloplacha.2011.03.004>
- Singh, Y. P., & Badruddin (2006). Statistical considerations in superposed epoch analysis and its applications in space research. *Journal of Atmospheric and Solar-Terrestrial Physics*, 68(7), 803–813. <https://doi.org/10.1016/j.jastp.2006.01.007>
- Skogseth, R., & Ellingsen, P. G. (2019a). Mooring data from the Isfjorden mouth – South (I-S) during 9 Sep 2010 to 3 Sep 2011 [Dataset]. *Norwegian Polar Institute*. <https://doi.org/10.21334/npolar.2019.b0e473c4>
- Skogseth, R., & Ellingsen, P. G. (2019b). Mooring data from the Isfjorden mouth – South (I-S) during 8 Sep 2011 to 3 Sep 2012 [Dataset]. *Norwegian Polar Institute*. <https://doi.org/10.21334/npolar.2019.2be7bdec>
- Skogseth, R., & Ellingsen, P. G. (2019c). Mooring data from the Isfjorden mouth – South (I-S) during 6 Sep 2012 to 28 Aug 2013 [Dataset]. *Norwegian Polar Institute*. <https://doi.org/10.21334/npolar.2019.a247e9a9>
- Skogseth, R., & Ellingsen, P. G. (2019d). Mooring data from the Isfjorden mouth – South (I-S) during 2 Sep 2013 to 26 Aug 2014 [Dataset]. *Norwegian Polar Institute*. <https://doi.org/10.21334/npolar.2019.6813ce6d>
- Skogseth, R., & Ellingsen, P. G. (2019e). Mooring data from the Isfjorden mouth – South (I-S) during 31 Aug 2014 to 24 Aug 2015 [Dataset]. *Norwegian Polar Institute*. <https://doi.org/10.21334/npolar.2019.11b7e849>
- Skogseth, R., & Ellingsen, P. G. (2019f). Mooring data from the Isfjorden mouth – South (I-S) during 31 Aug 2015 to 12 Aug 2016 [Dataset]. *Norwegian Polar Institute*. <https://doi.org/10.21334/npolar.2019.21838303>
- Skogseth, R., & Ellingsen, P. G. (2019g). Mooring data from the Isfjorden mouth – South (I-S) during 19 Aug 2016 to 2 Oct 2017 [Dataset]. *Norwegian Polar Institute*. <https://doi.org/10.21334/npolar.2019.cd7a2f7c>
- Skogseth, R., & Ellingsen, P. G. (2019h). Mooring data from the Isfjorden mouth – South (I-S) during 5 Oct 2017 to 25 Aug 2018 [Dataset]. *Norwegian Polar Institute*. <https://doi.org/10.21334/npolar.2019.54dc0d09>

- Skogseth, R., Olivier, L. L., Nilsen, F., Falck, E., Fraser, N., Tverberg, V., et al. (2020). Variability and decadal trends in the Isfjorden (Svalbard) ocean climate and circulation—An indicator for climate change in the European Arctic. *Progress in Oceanography*, *187*, 102394. <https://doi.org/10.1016/j.pocean.2020.102394>
- Stigebrandt, A. (1981). A mechanism governing the estuarine circulation in deep, strongly stratified fjords. *Estuarine, Coastal and Shelf Science*, *13*(2), 197–211. [https://doi.org/10.1016/s0302-3524\(81\)80076-x](https://doi.org/10.1016/s0302-3524(81)80076-x)
- Straneo, F., Hamilton, G. S., Sutherland, D. A., Stearns, L. A., Davidson, F., Hammill, M. O., et al. (2010). Rapid circulation of warm subtropical waters in a major glacial fjord in East Greenland. *Nature Geoscience*, *3*(3), 182–186. <https://doi.org/10.1038/ngeo764>
- Strzelewicz, A., Przyborska, A., & Walczowski, W. (2022). Increased presence of Atlantic water on the shelf south-west of Spitsbergen with implications for the Arctic fjord Hornsund. *Progress in Oceanography*, *200*, 102714. <https://doi.org/10.1016/j.pocean.2021.102714>
- Sundfjord, A., Albretsen, J., Kasajima, Y., Skogseth, R., Kohler, J., Nuth, C., et al. (2017). Effects of glacier runoff and wind on surface layer dynamics and Atlantic Water exchange in Kongsfjorden, Svalbard; a model study. *Estuarine, Coastal and Shelf Science*, *187*, 260–272. <https://doi.org/10.1016/j.ecss.2017.01.015>
- Svendsen, H. (1980). Exchange processes above sill level between fjords and coastal water. In *Fjord oceanography* (pp. 355–361). Springer.
- Svendsen, H., Beszczynska-Møller, A., Hagen, J. O., Lefauconnier, B., Tverberg, V., Gerland, S., et al. (2002). The physical environment of Kongsfjorden–Krossfjorden, an Arctic fjord system in Svalbard. *Polar Research*, *21*(1), 133–166. <https://doi.org/10.1111/j.1751-8369.2002.tb00072.x>
- Teigen, S. H., Nilsen, F., & Gjevik, B. (2010). Barotropic instability in the West Spitsbergen current. *Journal of Geophysical Research*, *115*(C7). <https://doi.org/10.1029/2009jc005996>
- Teigen, S. H., Nilsen, F., Skogseth, R., Gjevik, B., & Beszczynska-Møller, A. (2011). Baroclinic instability in the West Spitsbergen current. *Journal of Geophysical Research*, *116*(C7). <https://doi.org/10.1029/2011jc006974>
- Tverberg, V., Skogseth, R., Cottier, F., Sundfjord, A., Walczowski, W., Inall, M. E., et al. (2019). The Kongsfjorden transect: Seasonal and inter-annual variability in hydrography. In *The ecosystem of Kongsfjorden, Svalbard* (pp. 49–104). Springer.
- Vihtakari, M. (2020). PlotSvalbard: PlotSvalbard – Plot research data from Svalbard on maps [Software]. *R package version 0.9.2*. <https://github.com/MikkoVihtakari/PlotSvalbard>
- Vihtakari, M., Welcker, J., Moe, B., Chastel, O., Tartu, S., Hop, H., et al. (2018). Black-legged kittiwakes as messengers of Atlantification in the Arctic. *Scientific Reports*, *8*(1), 1–11. <https://doi.org/10.1038/s41598-017-19118-8>
- von Appen, W.-J., Beszczynska-Møller, A., & Fahrback, E. (2015). Physical oceanography and current meter data from mooring F3-15 [Dataset]. *PANGAEA*. <https://doi.org/10.1594/PANGAEA.853902>
- von Appen, W.-J., Latarius, K., & Kanzow, T. (2017). Physical oceanography and current meter data from mooring F3-16 [Dataset]. *PANGAEA*. <https://doi.org/10.1594/PANGAEA.870842>
- Walczowski, W., & Piechura, J. (2007). Pathways of the Greenland sea warming. *Geophysical Research Letters*, *34*(10). <https://doi.org/10.1029/2007gl029974>
- Walczowski, W., & Piechura, J. (2011). Influence of the West Spitsbergen current on the local climate. *International Journal of Climatology*, *31*(7), 1088–1093. <https://doi.org/10.1002/joc.2338>
- Wang, Q., Wekerle, C., Wang, X., Danilov, S., Koldunov, N., Sein, D., et al. (2020). Intensification of the Atlantic water supply to the Arctic Ocean through Fram Strait induced by Arctic sea ice decline. *Geophysical Research Letters*, *47*(3), e2019GL086682. <https://doi.org/10.1029/2019gl086682>
- Xie, J., Bertino, L., Counillon, F., Lisæter, K. A., & Sakov, P. (2017). Quality assessment of the TOPAZ4 reanalysis in the Arctic over the period 1991–2013. *Ocean Science*, *13*(1), 123–144. <https://doi.org/10.5194/os-13-123-2017>
- Zahn, M., Akperov, M., Rinke, A., Feser, F., & Mokhov, I. I. (2018). Trends of cyclone characteristics in the Arctic and their patterns from different reanalysis data. *Journal of Geophysical Research: Atmospheres*, *123*(5), 2737–2751. <https://doi.org/10.1002/2017jd027439>